Summer 2019

Reducing the Noise Impact of Unmanned Aerial Vehicles by Flight Control System Augmentation

Matthew B. Galles
Old Dominion University, matthew.galles@gmail.com

REDUCING THE NOISE IMPACT OF UNMANNED AERIAL VEHICLES BY FLIGHT CONTROL SYSTEM AUGMENTATION

by

Matthew B. Galles
A.S. August 2012, Tidewater Community College
B.S. December 2014, Old Dominion University

A Thesis Submitted to the Faculty of
Old Dominion University in Partial Fulfillment of the
Requirements for the Degree of

MASTER OF SCIENCE

MECHANICAL ENGINEERING

OLD DOMINION UNIVERSITY
August 2019

Approved by:
Brett Newman (Director)
Noah H. Schiller (Member)
Thomas E. Alberts (Member)

ABSTRACT

REDUCING THE NOISE IMPACT OF UNMANNED AERIAL VEHICLES
BY FLIGHT CONTROL SYSTEM AUGMENTATION

Matthew B. Galles
Old Dominion University, 2019
Director: Dr. Brett Newman

The aim of this thesis is to explore methods to reduce the noise impact of unmanned aerial vehicles operating within acoustically sensitive environments by flight control system augmentation. Two methods are investigated and include: (i) reduction of sound generated by vehicle speed control while flying along a nominal path and (ii) reduction of acoustic exposure by vehicle path control while flying at a nominal speed. Both methods require incorporation of an acoustic model into the flight control system as an additional control objective and an acoustic metric to characterize primary noise sources dependent on vehicle state. An acoustic model was developed based on Gutin's work to estimate propeller noise, both to estimate source noise and observer noise using two separate acoustic metrics. These methods can potentially mitigate the noise impact of unmanned aerial systems operating near residential communities.

The baseline flight control system of a representative aircraft was augmented with a control law to reduce propeller noise using feedback control of the commanded flight speed until an acoustic target was met, based on the propeller noise model. This control approach focuses on modifying flight speed only, with no perturbation to the trajectory. Multiple flight simulations were performed and the results showed that integrating an acoustic metric into the flight control system of an unmanned aerial system is possible and useful. A second method to mitigate the effects of noise on an observer was also pursued to optimize a trajectory in order to avoid an acoustically sensitive region during the path planning process. After the propeller noise model was incorporated into the vehicle system, simulations showed that it is possible to reduce the noise impact on an observer through an optimization of the trajectory with no perturbation to the flight speed.

ACKNOWLEDGMENTS

I would like to first thank my advisor, Dr. Brett Newman of the Dept. of Mechanical and Aerospace Engineering at Old Dominion University. The door to his office was always open when I needed his assistance and his enthusiasm about this project always gave me inspiration. It was encouraging that he supported the vision I had when it came to the direction of the research, but helped correct my course when he felt it necessary and guided me through difficult problems. I really enjoyed all of his classes and especially his sense of humor. Have I made it out of kindergarten or undergrad yet?

Thank you to Dr. Thomas Alberts for being on my committee, as well as many enjoyable conversations, discussions, and classes. It is because of him that I developed an initial interest in control systems.

I would also like to further thank my mentor at the NASA Langley Research Center, Dr. Noah H. Schiller for the countless discussions regarding the work, his assistance with the technical aspect of the research, and his edits on this thesis. His guidance when it came to becoming a better writer and researcher was invaluable and I could not have done this without him. For the technical content, he assisted me with learning acoustics, digital signal processing, and control systems. Additionally, I appreciate the fact that his door was always open for work discussions or lending an ear through difficult times.

There are many other colleagues I find it necessary to express my gratitude to, specifically: Dr. Kyle Pascioni, Dr. Steve Rizzi, for their guidance on the project, Mr. Kasey Ackerman, Dr. Irene Gregory, Dr. John Cooper, and Mr. Robert McSwain, for assistance with and information about the Greased Lightning-10 vehicle system, Dr. Randolph Cabell, for his feedback and discussions, Dr. Nikolas Zawodny for the data he acquired in the Structural Acoustics Loads and Transmission facility from which the energy consumption was derived and many excellent discussions, and Dr. Eric Greenwood, for his endless conversations regarding research, optimal control methods, life, boardgames, and many enjoyable conversations over Pad Thai. I would also like to acknowledge that this work was supported by the Revolutionary Vertical Lift Technology Project under the Advanced Air Vehicles Program in the National Aeronautics and Space Administration.

I would like to thank my mom, dad, and stepmom. My dad has always been my biggest supporter and I could not have come this far without his help. Lastly, I would like to thank my partner, Olechka, for being my cheerleader, number one fan, and best friend. You pushed me forward to the finish line, and for that, thank you.

TABLE OF CONTENTS

Page

LIST OF TABLES

LIST OF FIGURES

LIST OF SYMBOLS

Acronyms

AIAA	American Institute of Aeronautics and Astronautics
ANOPP	Aircraft NOise Prediction Program
CAD	Computer-Aided Design
CEAS	Council of European Aerospace Societies
DEP	Distributed Electric Propulsion
GL-10	Greased Lightning-10
NACA	National Advisory Committee for Aeronautics
NASA	National Aeronautics and Space Administration
PAS	Propeller Analysis System
PI	Proportional-Integral
RMS	Root Mean Square
SALT	Structural Loads and Transmission
SLUF	Straight-and-Level, Unaccelerated Flight
SPL	Sound Pressure Level
SWL	Sound Power Level
UAM	Urban Air Mobility
UAS	Unmanned Aerial System
UAV	Unmanned Aerial Vehicle
VTOL	Vertical Takeoff and Landing

Greek Symbols

$\boldsymbol{\lambda}(t)$	Lagrange multiplier	
χ	Heading angle	(deg)
μ	Constraint multiplier function	
ν	Flight velocity constraint	(m/s)
Ω	Propeller speed	(rad/s)
ω	Propeller speed	(rpm)
ω_n	Natural frequency of the system	(rad/s)
ρ	Density of air	(kg/m^3)
τ_s	Time constant	(s)
$\dot{\theta}$	Motor speed	(rpm)
ϑ	Directivity angle between observer propeller axis	(deg)
ζ	Damping ratio	

Roman Symbols

C	Constraint equation	
E	Total energy used	(J)
H	Hamiltonian	
J	Cost functional	
$J_{qn}(x)$	Bessel function of the first kind of order qn and argument x	
K_b	Saturation error gain, tuning parameter	(s^{-1})
K_i	Integral gain, tuning parameter	$(m/s^2 \cdot dB^{-1})$
K_p	Proportional gain, tuning parameter	$(m/s \cdot dB^{-1})$
Kv	Motor constant	(rpm/V)
L	Performance index process component or Lagrangian	
L_p	Sound pressure level	(dB re. 20 µPa)
L_W	Sound power level	(dB re. 10^{-12} W)
M	Mach number of the aircraft	
M_e	Mach number at an effective propeller radius	
$M_{\max}$	Maximum value allowed for $u_{sat}(t)$	(m/s)
$M_{\min}$	Minimum value allowed for $u_{sat}(t)$	(m/s)
M_t	Mach number of the propeller tip	
N	Number of propellers on the aircraft	
P_{disc}	$= T/\pi R_t^2$, Pressure loading on the propeller disc	(Pa)
P_m	Electrical motor power	(W)
Q	Propeller torque	(N m)
R_e	$= (0.7 - 0.8)R_t$, Effective propeller radius	(m)
R_t	Propeller tip radius	(m)
T	Propeller thrust	(N)
W	Sound power of propellers	(W)
W_0	$= 10^{-12}$ W, Reference sound power	(W)
c	Speed of sound in air	(m/s)
$\boldsymbol{c}(t)$	Roll and pitch rates from the path following controller	
$e_a(t)$	Acoustic error	(dB re. 10^{-12} W)
$\boldsymbol{f}(x, u)$	Constraint equations, $n \times 1$	
k	$= qn\Omega_1/c$, Acoustic wave number	
n	Number of propeller blades	
p_{rms}	Root-Mean-Square sound pressure at an observer	(Pa)
q	Harmonic index	
r	Distance from center of propeller rotation	(m)

$\boldsymbol{r}_a$	Position of the aircraft	(m)
$\boldsymbol{r}_{o/a}$	Position of the acoustic observer relative to aircraft	(m)
$r(t)$	Acoustic target, reference sound power level	(dB re. 10^{-12} W)
$r_a(t)$	Filtered acoustic reference	(dB re. 10^{-12} W)
$\boldsymbol{s_d}(t)$	$= [x(t), y(t), z(t)]$, Time-varying desired point	(m)
t_s	98% Settling time	(s)
$u(t)$	Unsaturated velocity command in the acoustic controller	(m/s)
$u_{sat}(t)$	Saturated velocity command in the acoustic controller	(m/s)
$\boldsymbol{u}(t)$	Flight dynamics controller output vector	
$\boldsymbol{u}$	Control or decision vector, $m \times 1$	
$\Delta v_a(t)$	Change in velocity command based on acoustic error	(m/s)
$\boldsymbol{v}_a$	Velocity vector of the aircraft	(m/s)
$v_c(t)$	Velocity command modified by acoustic controller	(m/s)
$v_n(t)$	Nominal velocity command, defined by mission requirements	(m/s)
x	$= kR\sin\vartheta$, Bessel function argument	
$\dot{\boldsymbol{x}}(t)$	System dynamic processes	
$\boldsymbol{x}$	State vector, $n \times 1$	
$y_a(t)$	Sound power estimate, output from acoustic model	(dB re. 10^{-12} W)
$\boldsymbol{y}(t)$	Flight properties vector, system output	

CHAPTER 1
INTRODUCTION AND BACKGROUND

Popularity of unmanned aerial systems (UAS) is on the rise, and as a result flight noise could become a major barrier to public acceptance. Therefore, control technologies may become necessary to mitigate noise impact during UAS operations. An interesting solution to overcome this barrier is the development of an acoustically-aware vehicle, which has the ability to modify where and how the aircraft flies to meet a noise requirement, as well as other mission requirements. This concept offers the potential to reduce noise exposure and enable widespread use of these vehicles in close proximity to people. This thesis seeks to provide a new method for mitigating the noise generated by these aircraft systems.

In this introductory chapter, a broad overview and a description of the motivation behind this research will be provided in §1.1. Then, a description of the problem specific to this current work will be reviewed in §1.2, followed by a review of the current literature in §1.3, and an outline of the chapters contained in this thesis will be provided in §1.4.

1.1 RESEARCH MOTIVATION AND DESCRIPTION

Noise from aircraft operation is an unwanted environmental effect in the aviation industry. The presence of noise – that is, unwanted sound – can lead to issues with learning in the classroom and childhood development, and also potentially lead to an increase in stress, which is associated with a myriad of unwanted and negative health problems.[1–4] As a result, acoustics is a highly researched field of study in aviation to reduce both the harmful effects of aircraft operation and to reduce the noise imposed on the general populace from the operation of commercial aircraft. In this section, some background information on noise in the aviation industry will be presented to motivate the current research.

1.1.1 Aviation Markets

In the aviation industry, several categories of aircraft operations exist: international, national, regional, and cargo operations. For all of these operations, various unique research topics of noise control require attention. One is noise that affects the populace, generally caused by the airframe or engine during takeoff and landing operations. Takeoff and landing noise can be mitigated via optimization of the thrust level and climb-turn profile during lift-off and departure, as well as approach to land.[5] Aircraft design is another means to noise mitigation. Considerable work has been done in propeller, compressor fan, nacelle, and intake-exhaust duct layout to reduce noise.[6–11]

Cabin noise is an issue for all airliners that support these markets (excluding cargo operations) and extensive research has been done to reduce or mitigate this noise to improve passenger comfort. This noise source, caused by the airframe interacting with air or the aircraft engines, is especially important in international flights due to the length of flight, and hence exposure period, and the previously mentioned health effects from noise in this scenario can be compounded.[12] Methods to reduce cabin noise range from using passive means to damp noise at high frequencies, active noise canceling using loudspeakers to produce a cancelling sound wave directly,[13,14] and actuators to vibrate the cabin shell to achieve the same effect.[15]

There exist additional specialized areas in which aerospace system noise has caused problems or been exploited that are mentioned here. First, sonic booms, or a high intensity traveling pressure wave generated from the shock waves present on an aircraft operating at supersonic conditions, can be disturbing and harmful to humans and animals. Supersonic commercial flight over the United States is banned for this reason. The literature contains a large body of past research on this topic, and a new generation of active research to reduce sonic boom intensity is ongoing.[16,17] Second, generated noise can be of such strength that harmful effects can even extend to the airframe itself. Acoustic loading on aircraft or helicopter structures generated from propeller or rotor blades, and acoustic loading on launch vehicle skin panels generated from rocket engines, are two notable examples.[18,19] Finally, attenuation of noise is not always the objective. Focused amplification of noise from aircraft on ground targets has been used as a psychological deterrent in hostile conflicts in the past.[20] However, a more commend trend is to exploit acoustic stealth.[21]

1.1.2 Urban Air Mobility Market

Urban Air Mobility (UAM) is a new addition to the commercial aviation portfolio that is quickly garnering interest by industry and the research community. The vehicles likely to support operations in this market are manned vertical takeoff and landing (VTOL) aircraft – vehicles that provide the flight capabilities of rotorcraft and may have interesting designs, such as distributed electric propulsion (DEP) systems that decouple the power source from the motors. DEP systems allow for novel aircraft designs that can result in a variety of benefits with regard to fuel efficiency, aerodynamics, and structural efficiency.[22–25] While there are many benefits to the use of these vehicles, the sound generated during operation could prove to be quite annoying, which will only intensify as more of these vehicles enter the airspace in and around communities. Research has shown that the psychoacoustic properties of rotor or propeller driven UAS may be more annoying than some other sources of everyday noise, such as delivery trucks.[26] Use of rotorcraft has been limited in the public sector due

to noise issues, which has been known for decades, and this will likely be a problem with UAS operation as the dominant noise source may be the rotors or propellers.[27,28] These manned aircraft can be used for a variety of missions and typically feature advanced control systems, and as a result, will most likely be supplemented by or replaced with UAS as autonomous flight technology matures. As this technology evolves, noise control strategies could be directly incorporated into flight control systems to reduce UAS noise.

Many benefits of noise control can be extended to the operation of UAS, starting with the reduction of noise that the general public experiences. This change could increase the use of UAS in everyday life, thus benefiting the aviation industry and consumers. Military capabilities could be increased by reducing noise generated. While there has been research performed to implement active noise canceling and passive noise damping, the focus of this work will be to incorporate an acoustic flight controller to reduce either the sound generated directly by modifying vehicle speed or to reduce the noise experienced by populated areas by way of path planning.

1.1.3 Urban Air Mobility Reference Vehicles

The vehicle concepts developed by industry are proprietary designs and therefore are not open for public research. Researchers at the National Aeronautics and Space Administration (NASA) created a number of reference vehicles for feasibility studies and other research. Work has been performed to study UAM conceptual designs, mission requirements, future research areas, operational optimizations, and human factors issues.[29–32] This subsection will describe a number of the reference vehicles developed, which is important because the vehicle model used in this current work is similar to one of the reference vehicles proposed for the UAM market.

Johnson, Silva, and Solis presented work outlining the design of three concept vehicles for use in the UAM market. The three designs, shown in Fig. 1.1, differ completely in payload capacity, aircraft type, and propulsion system.[33] The first is a quadrotor that can support a single passenger and has an electric propulsion system. The second is a six passenger transverse rotor helicopter that has a hybrid propulsion system. The third is a fifteen passenger tiltwing aircraft that has a cruise flight configuration with a turboelectric propulsion system and four rotors along the leading edge of the main wing. The main focus of the paper by Johnson et al. was to provide an overview of design implications for each of these vehicles and to discuss various research areas.

Reference [34] expands upon the work performed by Johnson et al. by including additional propulsion systems to the previously designed concept vehicles, as well as adding a new concept vehicle.[34] The new concept vehicle, shown as a computer-aided design (CAD)

Figure 1.1 Artistic Renditions of UAM Concept Vehicles

Figure 1.2 CAD Rendering of the Lift+Cruise Concept Reference Vehicle

rendering in Fig. 1.2, is a "Lift+Cruise VTOL Aircraft" and consists of eight rotors and one propeller, the latter acting as a pusher prop.[34] When operating during cruise flight, the rotors are inactive and the aircraft is only powered by the pusher prop. These concept designs will be referred to as reference vehicles, and are used at NASA in UAM vehicle research. A benefit of the new reference vehicle is that the acoustics are similar to a fixed wing aircraft during cruise flight.

1.2 PROBLEM STATEMENT AND OBJECTIVES

The following research question is now proposed: "How do we reduce aircraft noise at an observer by means of flight control system augmentation?" To answer this research question, this thesis will focus on a feasibility study in which two methods are investigated to reduce the amount of noise that observers are subjected to by the operation of UAS by means of flight control system augmentation. Investigations will be performed in simulation, using MATLAB Simulink,[35] to develop the control system and acoustic model, while utilizing a preexisting vehicle plant model of a UAS. The objectives of this feasibility study are indicated below.

1. Create logic to modify aircraft speed to modify propeller noise generation.
2. Demonstrate the feasibility of the concept of modifying the noise of a UAS through flight control system augmentation.
3. Formulate and integrate an acoustic requirement into the path planning of a UAS.
4. Create logic to modify the path of an aircraft to reduce the noise at an observer.

Objectives one and two are related to the first method of the feasibility study and objectives three and four are related to the second method of the feasibility study. Completing these objectives will result in a preliminary simulation of an acoustically-aware vehicle that could reduce the impact of some UAS noise on humans. This advancement could aide in reducing the barrier to acceptance by the general public to UAS, as the sound generated by these aircraft can be annoying. This aspect is especially important as these vehicles operate in a dense airspace close to populated areas.

1.3 LITERATURE REVIEW

First, a review of literature related to the noise models developed for this thesis will be presented. Then, a sample of the literature related to optimization techniques used in this work will be discussed. Recent work performed to achieve a goal of reducing noise at an observer will be compared and contrasted to the current work.

1.3.1 Propeller Noise

Lev Yakovlevich Gutin's initial research on propeller noise was originally published in 1936 in a Russian journal and a translated version was released in a German publication in the same year. The National Advisory Committee for Aeronautics (NACA) translated Gutin's work into English and released it as a technical memorandum in 1948.[36] As Ffowcs Williams and Hawkings have mentioned, Gutin was the first to provide a theoretical study of two-bladed propeller noise.[37] Gutin theoretically derived what is known as "Loading Noise" but some researchers refer to it simply as "Gutin Noise". Gutin noise is simply the steady loading force component of the dipole term of the Ffowcs Williams-Hawkings equation, which models sound as a result of the aerodynamic loading of the wing or propeller blade.

Gutin's work forms the basis for both the source noise and observer noise acoustic models used in this work. A few assumptions and limitations are inherent with his work, some of which were corrected by later works. The first limitation is that Gutin only considers loading noise and does not take into account the effect of thickness noise. Another limitation

is that Gutin does not account for angle of attack, which can have an effect on the acoustics of the propeller as the loading goes from a steady to an unsteady loading condition.[38] The third limitation is that Gutin's theory does not account for forward flight speed, so the propeller is assumed to be in a zero velocity flow state. The effects of forward flight speed on sound propagation were added to this theory by Garrick and Watkins in 1954.[39] Regardless of these limitations, Gutin's approach is acceptable for the initial concept of the work contained within this thesis.

1.3.2 Optimization

The optimization techniques employed in the second half of this work are heavily based on "Applied Optimal Control: Optimization, Estimation and Control" by Bryson and Ho.[40] The introductory chapter of the text outlines static optimization techniques, with the subsequent chapters presenting optimization problems of dynamic systems with and without state constraints. The current work aims to build upon the foundation laid in Chapters 2 and 3 of Bryson and Ho, culminating in work that considers a state constraint on velocity while avoiding an acoustically sensitive observer.

Falck et al. wrote a paper as an initial study in optimizing quadrotor trajectories using gradient based optimization techniques.[32] Their work coupled a six degree of freedom quadrotor model with an acoustic monopole source to track the SPL perceived by a ground observer during a flyover. They were able to create trajectories that considered limits placed on the SPL experienced by an observer. While some of the objectives between this current work and Falck et al. coincide, it is important to note some of the assumptions differ with regards to the acoustic model employed. The current work incorporates an analytical model based on loading noise with varying sound power into the trajectory optimization, as opposed to a theoretical monopole source model of constant sound power. Another key difference is that indirect optimization techniques are used in the current work, where Falck et al.[32] used direct optimization techniques.

Greenwood proposed a method for rotorcraft trajectory optimization that is suitable for dynamic replanning – inspired by similar research in robotics, unmanned aerial vehicle (UAV), and autonomous ground vehicles.[41–44] Similar to the current work, Greenwood's objective was to optimize the path of a rotorcraft around acoustically sensitive areas according to some defined acoustic cost. In contrast to the current work, Greenwood's approach does not use a traditional, computationally expensive optimization method, but rather employs a combinatorial optimization technique. First, a large database of rotorcraft maneuver segments was generated and an associated acoustic cost for each segment was calculated using a semiempirical noise model.[45] Then, individual maneuver segments were combined

based on the total acoustic cost to form an optimal flight path. The main benefit of this method over the current work is that it is computationally cheap – enabling near real time dynamic replanning – but the optimality of the solution is constrained by the discretized nature of the technique.

1.4 THESIS OUTLINE

The thesis is organized in the following chapters. Chapter 2 describes the vehicle system, beginning with the vehicle system model that was developed by the Dynamic Systems and Control Branch at the NASA Langley Research Center. The vehicle system includes the plant model created to develop the flight control system, the guidance system, and the autopilot control laws. Additionally, an open-loop energy consumption model will be discussed.

Chapter 3 covers aspects of the research related to acoustics. Efforts to model the noise, both at the source, and at an observer, will be presented along with the appropriate sound metrics and a description of the Simulink[35] implementation.

The development of a speed augmentation control law for an acoustically-aware vehicle will be covered in Chapter 4. Operation of the vehicle plant model in conjunction with the source noise model developed in Chapter 3 will be discussed as well as the integration of the acoustics model with the aforementioned control law. Results of simulations performed to validate the work will be discussed and presented.

The final objective of the current work, optimizing a flight trajectory, will be covered in Chapter 5, and will cover aspects of optimal control and path planning. The development of an optimal control law and its integration into the vehicle plant model will be covered, and simulations will be analyzed for effectiveness.

Conclusions and future work will be discussed in Chapter 6.

CHAPTER 2
VEHICLE SYSTEM

This chapter will give a brief overview of the vehicle system used to develop the control law presented later in Chapter 4.

The vehicle system, as the term is used here, comprises a vehicle plant model, a guidance system, and an autopilot system, all three of which were provided by the Dynamic Systems and Control Branch at the NASA Langley Research Center. While they were not developed by the author, they are described here to provide background for this contribution. In Fig. 2.1, the guidance system is shown as a path-following controller, the autopilot is represented by a flight dynamics controller, and the plant model is represented by the vehicle dynamics model. After these systems are described, an energy consumption model will be presented that was developed by the author to analyze energy consumption during simulations.

2.1 VEHICLE DYNAMICS MODEL DESCRIPTION

The research question posed in this thesis is largely motivated by an increased interest in the UAM market, and thus it would be useful to use a vehicle model that is representative of one of the four UAM reference vehicles[33,34] previously introduced in the literature review. An aircraft model and accompanying flight control system for a vehicle called the Greased Lightning-10 (GL-10)[46,47] was available for use, and as an added benefit, it was representative of the tiltwing rotor reference vehicle proposed[33] for the UAM market.

Development of the GL-10 began in 2013 as an initial study of four different VTOL vehicle concepts.[48] After the initial study was completed, development continued with wind tunnel testing of a 50% scale build of the GL-10, creation of a vehicle system model for flight controls development, and concluded with flight tests in 2017.[46,47]

Figure 2.2 shows a CAD rendering of the GL-10 in a cruise flight configuration with eight motors mounted to the wings and two motors mounted to the horizontal stabilizers, with each motor driving a propeller. The GL-10 is a VTOL aircraft and has a DEP system in a tilt-rotor configuration with ten rotors, so it is capable of both cruise flight and hover flight. However, only the cruise flight configuration will be considered for this work.

A vehicle dynamics model was previously created for the GL-10 flight controls development and will be used in this study. This model embodies the differential equations governing the flight dynamics of the vehicle, with aerodynamic coefficients determined from wind tunnel testing. Equations of motion governing the GL-10 flight dynamics were derived based on

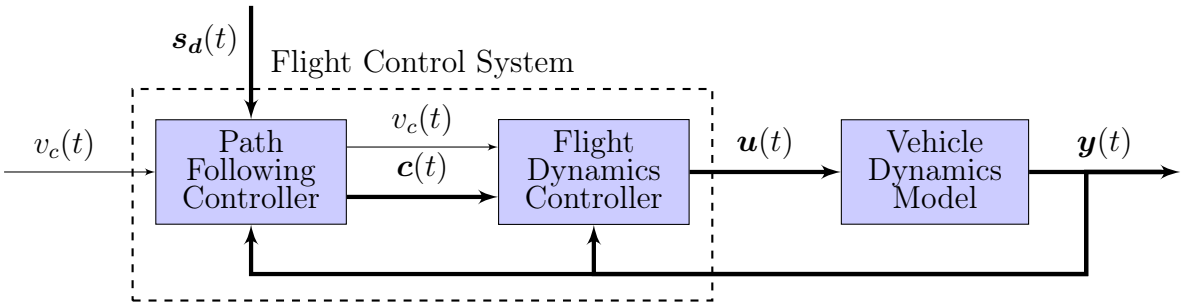

Figure 2.1 Block Diagram of the Vehicle System

the work of Murphy et al.[49] The vehicle dynamics model output, $\boldsymbol{y}(t)$, is comprised of the vehicle attitude, roll, pitch, and yaw rates; the vehicle position, velocity, and acceleration; and the individual speeds, thrusts, and torques of all GL-10 propellers. The latter three outputs are used in the source noise model, as will be shown later, and the other signals in the vehicle dynamics output are fed back into the path-following and flight dynamics control laws.

2.2 PATH-FOLLOWING CONTROLLER DESCRIPTION

The path-following controller is a guidance system that implements the approach proposed by Cichella et al. to steer a UAV along a proposed trajectory.[50,51] As shown in Fig. 2.1, a nominal path, $\boldsymbol{s_d}(t)$, is provided, along with a speed profile, $v_c(t)$, for the UAV to follow. With this approach, the controller attempts to follow this trajectory without a temporal constraint. This strategy leaves the vehicle speed as a degree of freedom,[1] in contrast to some other tracking systems in which the trajectory is defined, not simply a nominal path. Another benefit to this method is that it uses the special orthogonal group in three dimensions, also known as rotation group SO(3), when formulating the attitude relationships.[50] In doing this, the formulation creates a control law that avoids the singularities present in Euler-angle formulations, thus ensuring a singularity-free control law.[50,51] Another approach would be to use the switching strategy described in Ref. [52]. The output of the path-following controller is comprised of the commanded roll and pitch rates, $\boldsymbol{c}(t)$, and the input velocity command, $v_c(t)$, which can be saturated to ensure that it does not drop below the stall speed of the GL-10.

[1]This is why the vehicle speed must be specified via a speed profile, $v_c(t)$, for the path-following controller.

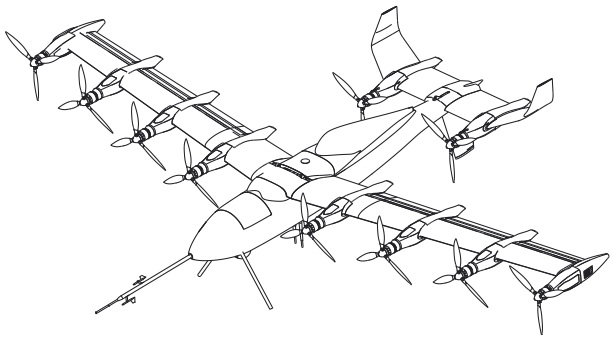

Figure 2.2 GL-10 Prototype in a Cruise Flight Configuration

2.3 FLIGHT DYNAMICS CONTROLLER DESCRIPTION

The flight dynamics controller is a rate-tracking autopilot designed using classical control techniques and uses a proportional-integral (PI) rate-tracking control law with an $\mathcal{L}_1$ adaptive augmentation.[53–55] The inputs to the flight dynamics controller are the velocity command and commanded roll and pitch rates from the guidance system, from which the flight dynamic controller creates a set of control surface commands, $\boldsymbol{u}(t)$, to be sent to the vehicle plant model. After achieving stable flight by manually tuning the static PI gains, an $\mathcal{L}_1$ adaptive controller augments the baseline PI controller to provide robustness in the presence of uncertain aerodynamics during the transition from hover to forward flight and account for other model uncertainties. $\mathcal{L}_1$ adaptive control was chosen for this application due to its proven ability to provide predictable, repeatable performance in the presence of abnormal or extreme flight conditions.[56] Additionally, $\mathcal{L}_1$ adaptive control allows for fast adaptation with guaranteed robustness by decoupling the adaption timescale from robustness to model uncertainty.[55] More information on $\mathcal{L}_1$ adaptive control can be found in work performed by Xargay et al. and Hovakimyan et al.[54,55]

2.4 ENERGY CONSUMPTION MODEL DEVELOPMENT

The fourth component in the vehicle system, shown in Fig. 2.3, is an energy consumption model that can be used to evaluate the operating efficiency of the vehicle with and without acoustic control. Energy consumed could be a performance parameter in the future, and implementation of the energy consumption model allows for analysis of this during a mission. Thus, the total energy used will serve as the metric for comparison of electrical efficiency between operating states.

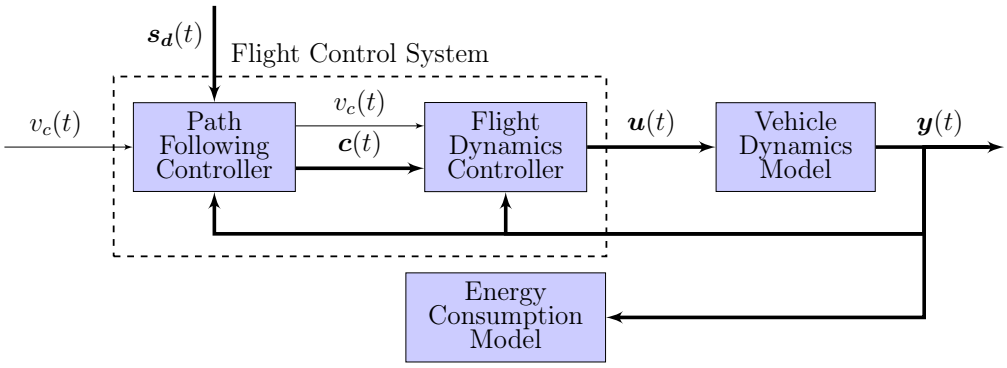

Figure 2.3 Block Diagram of the Vehicle System with Energy Consumption Model

The model is based on data[2] collected during an experiment in the anechoic chamber within the Structural Acoustics Loads and Transmission (SALT) facility at the NASA Langley Research Center. This test was conducted to characterize the sound generated by a three-bladed, 16.0" diameter folding propeller, driven by a 360 Kv[3] motor, at various motor speeds. This motor and propeller combination was used on the GL-10. Results from the experiment are presented in Tab. 2.1.

A regression analysis was performed on motor speed and power in Tab. 2.1 to create a model of the power consumption, given as

$$P_m = 4.867 \times 10^{-5}\dot{\theta}^2 - 0.1991\dot{\theta} + 249.0\,, \tag{2.1}$$

in which P_m is the estimated power in Watts consumed by the motor, and $\dot{\theta}$ is the motor speed in rpm. During the GL-10 simulations, the power consumption for each motor at each time step was computed using Eq. (2.1). The wing and tail power consumptions were integrated with respect to time over the duration of the simulation and summed to calculate the total energy used during the mission, given by

$$E = \sum_{n=1}^{8} \int_0^{t_f} P_{Wing_n} dt + \sum_{n=1}^{2} \int_0^{t_f} P_{Tail_n} dt\,. \tag{2.2}$$

Equation (2.2) is the proposed energy consumption model, in which E is the energy used in Joules. Accounting for the wing and tail motors separately is important as the flight dynamics controller sends separate thrust commands to the wing and tail motors.

[2]Provided by Dr. Nikolas Zawodny of the Aeroacoustics Branch at the NASA Langley Research Center.
[3]The Kv rating relates the motor speed (rpm) to the motor voltage (V).

Table 2.1 Propeller Speed and Power Recorded During GL-10 Motor Testing

$\dot{\theta}$ (rpm)	Power (W)	Voltage (V)	Current (A)
2006	35	5.6	6.2
2500	61	7	8.8
3005	100	8.4	11.9
3510	157	9.8	16.1
4006	233	11.2	20.9
4510	333	12.6	26.5
5011	465	13.9	33.3
5519	625	15.4	40.7
6004	820	16.7	49.1

2.5 SUMMARY

In this chapter, a review of the physical vehicle system was provided. This review included a description of the GL-10 aircraft and the vehicle dynamics model that was created to simulate flight of the GL-10 for controls development. Additionally, descriptions of the flight dynamics controller and the path-following controller were provided, and details of an energy consumption model that was created for this work was included. These systems will be instrumental in developing the speed augmentation acoustics controller in Chapter 4.

CHAPTER 3
NOISE MODELS

In this chapter, two acoustic models will be developed that are necessary to create an acoustically-aware vehicle. The first acoustic model will be a source noise model, used to estimate the sound power level of a UAS during flight. This model will be referred to as the Source Sound Power Model and will be used to develop the control law to reduce the sound power level generated by the vehicle. The second model will be an observer noise model, which will be used to provide an estimate of the sound pressure level that an observer is experiencing as a UAS operates through a flight segment of a mission. This model will be referred to as the Observer Sound Pressure Model and will be used to optimize a flight trajectory so that the UAS can avoid areas that are potentially sensitive to noise.

First, some background information regarding steady loading noise will be discussed in §3.1. Then, the Source Sound Power Model to be used in Chapter 4 will be developed in §3.2, followed by the development of the Observer Sound Pressure Model to be used in Chapter 5 in §3.3. Lastly, the chapter will conclude with a summary in §3.4.

3.1 PROPELLER STEADY LOADING NOISE

3.1.1 Background

Although limited in complexity, the Gutin equation is a good candidate for a low fidelity model as it has been shown to provide good results for the first few harmonics.[57] Additionally, the Gutin equation is an analytical model that can easily be implemented in simulation.

Certain limitations require consideration when using the Gutin formula. Gutin stated that this model should only be used for stationary noise estimation without forward flight, however, literature suggests that it can be acceptable for low speed forward flight when the vehicle speed is small compared to the speed of sound.[58] Additional steady sources of noise that are not considered in the Gutin formulation are thickness noise, arising from the displaced air and nonlinear quadrupole terms, arising from nonviscous flow near the surface of the propeller blade.[59]

3.1.2 Implementation

Notation adopted by both Gutin[36] and Deming[57] will be used for the sound pressure equation. First, Gutin gives the root mean square (RMS) pressure at a far field observer as

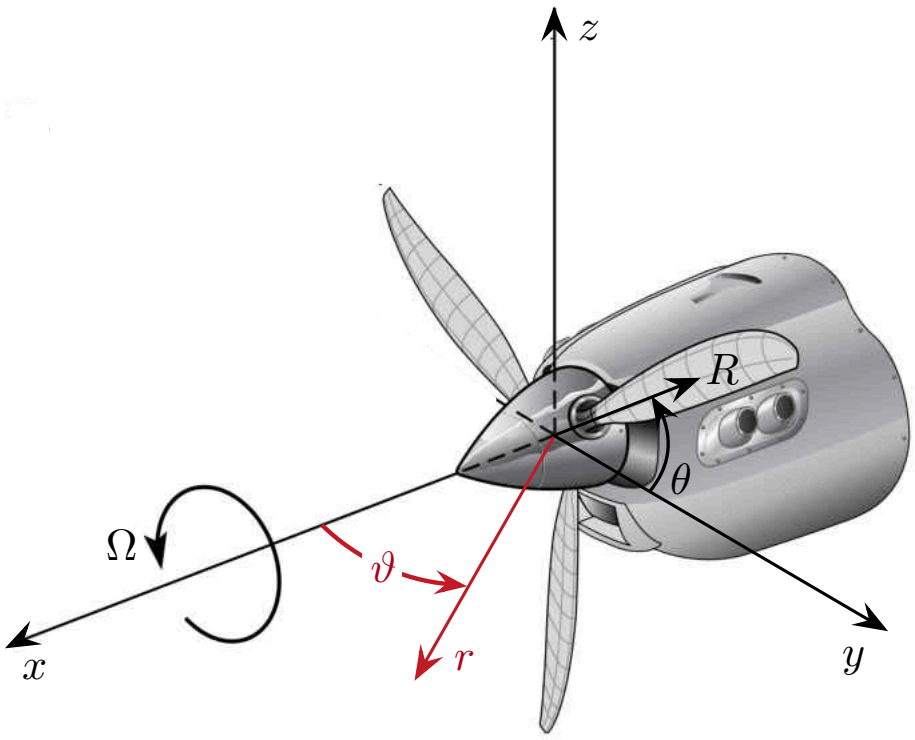

Figure 3.1 Gutin Model Propeller Geometry

$$p_{rms}(\Omega, r, T, Q, \vartheta) = \frac{qn\Omega}{2\sqrt{2}\pi cr}\left|-T\cos\vartheta + Q\frac{c}{\Omega R_e^2}\right| J_{qn}\left(kR_e\sin\vartheta\right) , \tag{3.1}$$

in which p_{rms} is the RMS pressure, q is the harmonic index, n is the number of propeller blades, Ω is the propeller speed in rad/s, c is the speed of sound, r is the distance from the center of the propeller to the observer, T is the propeller thrust, ϑ is the directivity angle from the axis of rotation in radians, Q is the torque applied to the propeller, R_e is the effective propeller radius and is equal to $0.8R_t$, in which R_t is the full tip radius of the propeller. $J_{qn}\left(kR\sin\vartheta\right)$ is the Bessel function of the first kind and k is the acoustic wavenumber. Figure 3.1, modified from Zorumski and Weir,[60] shows that the propeller rotates about the x-axis at a rate of Ω, r lies in the x-y plane at an angle ϑ away from the x-axis, and θ lies in the azimuthal plane, in which positive θ is in the direction of the propeller rotation.

Necessary for the Bessel argument in Eq. (3.1) is the acoustic wavenumber k, defined as

$$k = \frac{qn\Omega}{c} . \tag{3.2}$$

From Eq. (3.1), observe that steady loading noise is highly dependent on the propeller speed,

Table 3.1 Reference Conditions Used to Estimate Sound Pressure as a Function of Directivity Angle

Parameter	Variable	Units	Value
Harmonic index	q	-	1
Number of propeller blades	n	-	2
Propeller speed	Ω	rad/s	178.0
Speed of sound	c	m/s	343
Distance to observer	r	m	25.9
Propeller thrust	T	N	2971.4
Propeller torque	Q	N m	340.3
Propeller tip radius	R_t	m	1.45
Propeller effective radius	R_e	m	1.09

thrust, and torque. The SPL, L_p, is given by

$$L_p = 20 \log_{10} \left(\frac{p_{rms}}{p_0} \right) , \tag{3.3}$$

in which p_0 is a reference pressure[1] of 2×10^{-5} Pa.

The loading noise predicted by the Gutin model is comprised of two components, one related to propeller thrust and the other related to propeller torque. The thrust term, $-T \cos \vartheta$, is a function of propeller thrust and directivity angle. The torque term, $Qc/\Omega R_e^2$, is a function of propeller torque, sound speed, propeller speed, and effective propeller radius. As a validation exercise, the reference conditions from Deming[57], listed in Tab. 3.1, were used to calculate each component of sound pressure and the results are presented in Fig. 3.2. First, the sound pressure due to torque is presented with a purple dash-dot line, which resembles a rose flower plot with only two petals. Note that the loading noise due to torque is positive for all directivity angles for the acoustic model used. Next, the sound pressure due to thrust is presented in dashed blue and red, resembling a rose flower plot with four petals. Since the thrust term depends on the cosine of the directivity angle, it is negative for directivity angles $0° \leq \vartheta < 90°$ and $270° < \vartheta \leq 360°$, which is shown in dashed red. In dashed blue, the pressure due to thrust is positive for directivity angles $90° \leq \vartheta < 270°$. Finally, the summation of the torque and thrust noise are presented in solid blue (for positive pressure) and solid red (for negative pressure). One can see a maximum value at about 120° and a secondary maximum at about 45°. The torque reduces the pressure amplitude due to thrust in front of the propeller, from $\vartheta = 270°$ to 0° and from $\vartheta = 0°$ to 90°, and increases

[1] A common reference pressure for calculating sound pressure level is 2×10^{-5} Pa, which is the threshold of human hearing.[61]

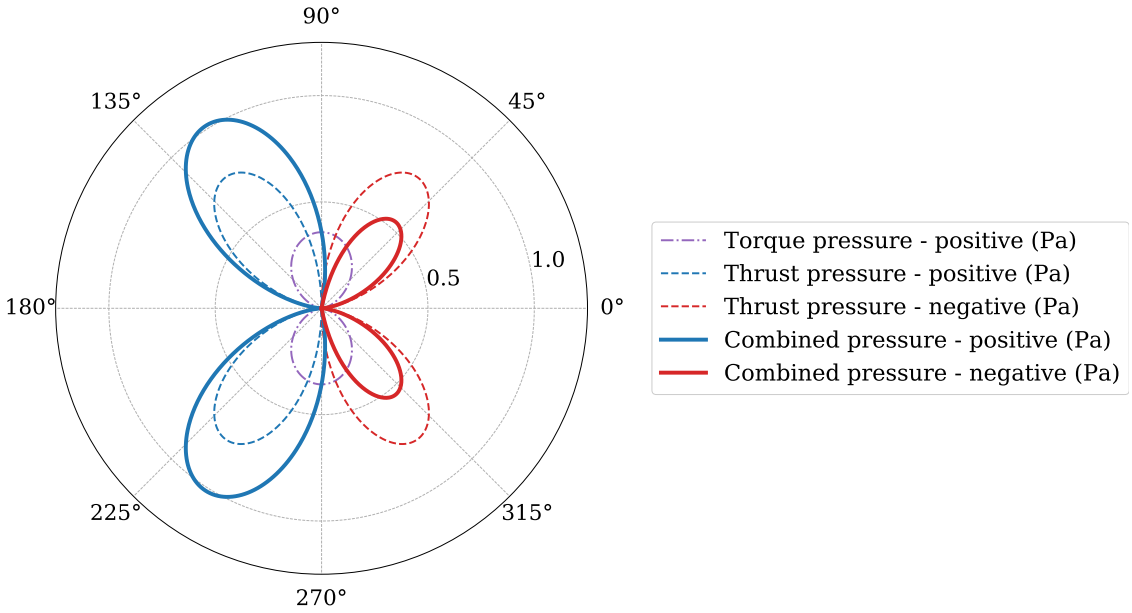

Figure 3.2 Sound Pressure Amplitude vs. Directivity Angle, ϑ, Considering Torque, Thrust, and Both

the pressure amplitude behind the propeller from $\vartheta = 90°$ to $270°$.

3.2 SOURCE SOUND POWER MODEL DEVELOPMENT

In this feasibility study, a model to describe source noise and an appropriate sound metric are necessary to incorporate an acoustic target into the flight control system. In the preceding section, RMS pressure was calculated, but the sound metric will instead be sound power level. This section will provide a brief background of the Source Sound Power Model, the sound metric, and its implementation.

3.2.1 Implementation

The Source Sound Power Model used in this study estimates the total radiated sound power level of the vehicle and is based on the Gutin model described in the preceding section.[36] To develop a model for total sound power of a propeller, it is necessary to relate sound pressure to sound power. Therefore,

$$W = \int_0^{\pi} \frac{p_{rms}^2}{\rho c} 2\pi r^2 \sin\vartheta d\vartheta \,, \tag{3.4}$$

in which ρ is the density of air and W is the sound power of the propeller. Substituting Eq. (3.1) into Eq. (3.4) and rearranging yields

$$W = \frac{q^2 n^2 \Omega_1^2}{2\pi\rho c^3} \int_0^\pi \left| -T\cos\vartheta + Q\frac{c}{\Omega R_e^2} \right|^2 J_{qn}^2 \left(kR_e \sin\vartheta\right) \sin\vartheta d\vartheta \,. \tag{3.5}$$

Since it is difficult to develop a closed-form solution for Eq. (3.5), the sound power is numerically integrated and updated at every time step during simulation. This model is a function of propeller speed, thrust, and torque, which are values easily extracted from the GL-10 simulation. Assuming the acoustic sources are incoherent or have no stable phase relationship, the total sound power, W_{Total}, is

$$W_{Total} = 8W_{Wing} + 2W_{Tail} \,, \tag{3.6}$$

in which W_{Wing} is the sound power of a single wing propeller and W_{Tail} is the sound power of a single tail propeller. Computing the total sound power level (SWL) from Eq. (3.6) results in

$$L_{W,\,Total} = 10\log_{10}\left(\frac{W_{Total}}{W_0}\right) \,, \tag{3.7}$$

in which L_W is the total radiated SWL and W_0 is the reference power, 10^{-12} W.

3.2.2 ANOPP-PAS Based Surrogate Model

Noise estimates from the Gutin model can be validated using the Propeller Analysis System (PAS) of the Aircraft Noise Prediction Program (ANOPP) since ANOPP-PAS estimates have been shown to agree well with experimental results.[60,62] ANOPP-PAS can predict noise levels for propeller aircraft based on the propeller geometry and operating state, atmospheric conditions, and geometry between the noise source and receiver. The software does this by implementing Farassat's Formulation 1A, which is a solution of the Ffowcs Williams-Hawkings equation.[37,63–65] Detailed information on ANOPP-PAS can be found in a readily available user's guide.[66] The efficacy of the Gutin noise model, presented in Eqns. (3.5), (3.6), and (3.7), will be evaluated using a surrogate model developed using ANOPP-PAS.

The surrogate acoustic model implemented uses a one-dimensional lookup table relating propeller speed to total radiated sound power level. Propeller loading noise, which is assumed here to be the dominant contributor to radiated sound power for the forward flight condition, is proportional to the propeller tip speed. As there are ten multibladed propellers on the GL-10, it is assumed that the propeller rotational velocities are equivalent for the acoustic

Table 3.2 Total Radiated Sound Power Level and Associated Parameters Used in Simulation

		Simulation		
Parameter	Units	1	2	3
True air speed	m/s	21.3	26.5	31.1
Altitude	m	30.5	30.5	30.5
Propeller speed	rpm	6811.0	8223.0	9629.0
Wing prop in-flow angle	deg	9.3	4.6	2.4
Tail prop in-flow angle	deg	4.3	0.4	2.6
PAS thrust	N	30.1	41.9	56.0
PAS torque	N m	1.2	1.7	2.6
$L_{W,\,\mathrm{PAS}}$	dB (ref. W_0)	112.3	119.9	127.7
$L_{W,\,\mathrm{Gutin}}$	dB (ref. W_0)	110.1	118.5	125.6

prediction. This lookup table approach allowed for swift implementation and integration with the flight control system to provide a proof of concept and validation of the Gutin model.

Three forward flight speeds were chosen based on the operational capacity of the vehicle for these simulations: 21.3, 26.5, and 31.1 m/s. The lowest velocity command, 21.3 m/s, was the slowest that the vehicle could fly in simulation while configured as a traditional fixed-wing aircraft. Conversely, the highest velocity command, 31.1 m/s, was the fastest flight speed the vehicle could achieve, limited by the capability of the motors. A flight speed of 26.5 m/s was chosen to provide a medium point for the lookup table. Using these velocity commands, simulations of the GL-10 operating in straight-and-level, unaccelerated flight (SLUF) were performed in Simulink[35] to acquire operating conditions at steady state. The parameters presented in Tab. 3.2 were acquired as output of the simulation.

The specific configuration in Tab. 3.2, along with three dimension coordinates to create a sphere of radius 2.4 m (12 blade radii) around a noise source, were used to create an input deck for ANOPP-PAS.[67] The radius was chosen so that calculations were performed in the far field, thus ensuring a proper comparison between the Gutin and ANOPP-PAS models. Then, ANOPP-PAS was used to estimate the sound pressure at the points along the surface of the sphere around the acoustic source. The sound pressure fields were then integrated to calculate the individual propeller sound powers, then summed to calculate the total vehicle sound power levels shown in the second to last row of Tab. 3.2. Estimates of thrust produced by the propeller and torque exerted on the propellers were extracted from the PAS output results, which were used as inputs to the Gutin model for comparison.

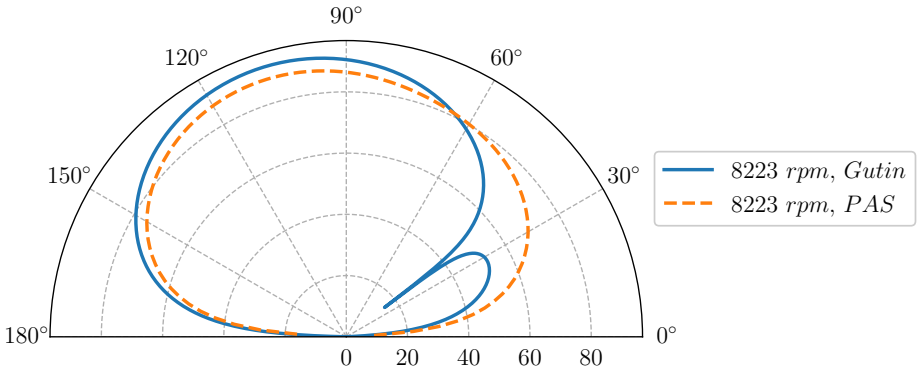

Figure 3.3 Sound Pressure Level vs. Directivity Angle,
Generated Using Gutin and ANOPP-PAS

3.2.3 Comparison of Gutin and ANOPP-PAS Models

Figure 3.3 shows a comparison between the SPL estimated by the Gutin model, Eq. (3.3), and ANOPP-PAS based on a radius of 2.4 m and a propeller speed of 8223 rpm. Similar trends are shown between both SPL curves in Fig. 3.3 except near a directivity angle of 30°. In this region, the Gutin model under predicts sound pressure level when compared to the PAS model. It is not expected that Gutin and PAS will match perfectly, as Gutin omits some acoustic sources that PAS includes. The Gutin model does not consider propeller in-flow angle and models only loading noise, so thickness noise, quadrupole terms, and nondeterministic sound sources are not considered. Also, the Gutin model does not account for blade geometry, which is modeled in ANOPP-PAS. These differences between the Gutin model and ANOPP-PAS may contribute to the sound power level errors shown in the last row of Tab. 3.2 and in Fig. 3.3. The error seems to be consistent (a bias of approximately 2 dB) for all three conditions. Based on these results, Gutin is an acceptable model for this feasibility study because it adequately captures the change in radiated sound power and sound pressure due to changes in vehicle operating state.

3.3 OBSERVER SOUND PRESSURE MODEL DEVELOPMENT

In the previous section, a model was developed that will be used to incorporate acoustics into the flight control system of the aircraft model. In this section, a model will be developed that will be used to incorporate acoustics in the path-planning process. To do this, a point mass optimal control simulation will be developed in Chapter 5 to create the trajectory that the aircraft will fly on. In this point mass simulation, the thrust and torque terms are not available and as a result, another form of Gutin pressure will be used for incorporating the Observer Sound Pressure Model into the point mass simulation. This engineering form is

independent of propeller torque and, based on Theodorsen and Regier[58], is

$$p_{rms} = \frac{P_{\text{disc}}}{2\sqrt{2}} \frac{R_t}{r} M_t \left(\frac{M}{M_e^2} - \cos\vartheta \right) qnJ_{qn} \left(qnM_e \sin\vartheta \right) , \tag{3.8}$$

with the propeller disc pressure given as

$$P_{\text{disc}} = \frac{T}{\pi R_t^2} , \tag{3.9}$$

in which T is the thrust generated by the propeller, R_t is the tip radius of the propeller, r is the distance to the observer, M_t is the Mach number of the propeller tip, M is the Mach number of the vehicle, M_e is the Mach number of the effective propeller radius (typically given as 0.7-0.8R_t), q is the harmonic index, and n is the number of propeller blades. A lookup table created from wind tunnel testing of the GL-10 was used to interpolate the propeller thrust based on angle of attack (assumed to be zero), aircraft velocity, and propeller speed. The propeller speed was calculated using

$$\omega = 60 \frac{|\boldsymbol{v}_a|}{2R_t J} , \tag{3.10}$$

in which ω is the propeller speed in revolutions per minute and J is the advance ratio, assumed to be 0.6 based on a propeller efficiency of 80%.[67] The directivity angle, ϑ, is calculated using the dot product,

$$\vartheta = \arccos \frac{\boldsymbol{v}_a \cdot \boldsymbol{r}_{o/a}}{|\boldsymbol{v}_a| \left| \boldsymbol{r}_{o/a} \right|} , \tag{3.11}$$

in which $\boldsymbol{v}_a$ is the velocity vector of the aircraft, given by

$$\boldsymbol{v}_a = [\, \dot{x}(t) \;\; \dot{y}(t) \;\; \dot{z}(t) \,] , \tag{3.12}$$

and is in the inertial frame, in line with the propeller's axis of rotation. The relative position of the observer to the aircraft, $\boldsymbol{r}_{o/a}$, comes from

$$\boldsymbol{r}_o = \boldsymbol{r}_a + \boldsymbol{r}_{o/a} , \tag{3.13}$$

in which $\boldsymbol{r}_o$ is the position of the observer and $\boldsymbol{r}_a$ is the position of the aircraft. Thus,

$$\boldsymbol{r}_{o/a} = \boldsymbol{r}_a - \boldsymbol{r}_o . \tag{3.14}$$

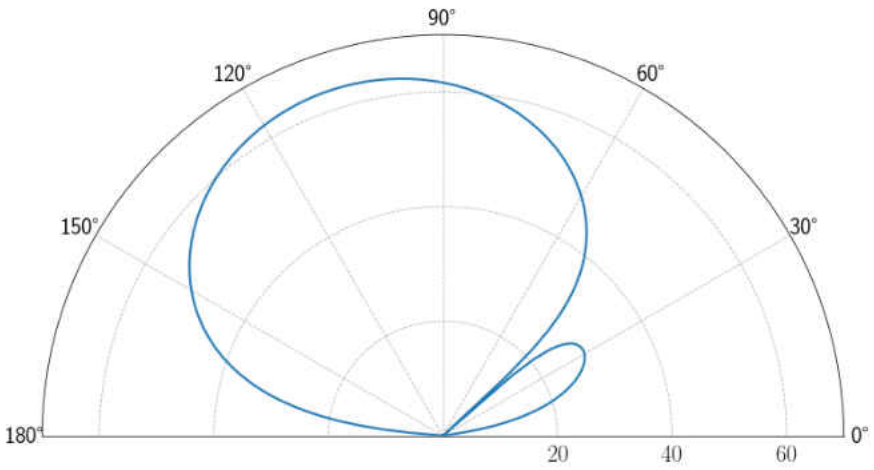

Figure 3.4 Sound Pressure Level vs. Directivity Angle Between the Propeller Axis and the Observer

Additionally, taking the norm of $\boldsymbol{r}_{o/a}$ yields the distance to the observer from the center of the propeller, r. Shown in Fig. 3.4 is a polar plot of the SPL experienced by an observer 2 m away from the propeller of an aircraft flying at 30 m/s.

In order to provide a conservative estimate of SPL experienced by the observer, the angle at which maximum SPL occurs was used. This modification also reduces computation time and simplifies the observer noise model. To simplify the estimated RMS pressure, uniform directivity was assumed at the maximum SPL shown in Fig. 3.4, which was 108°, or 0.6π rad. Incorporating this into Eq. (3.8) results in

$$p^*_{rms} = \frac{P_{\text{disc}}}{2\sqrt{2}} \frac{R_t}{L} M_t \left(\frac{M}{M_e^2} - \cos 0.6\pi \right) qnJ_{qn} \left(qnM_e \sin 0.6\pi \right) . \tag{3.15}$$

The acoustic model provides an estimate of the SPL, L_p, experienced by the observer as a result of one propeller on the GL-10 using Eq. (3.3).

As the acoustic sources are presumed to be incoherent, meaning that they have random phase and do not have constructive or destructive interference between the waves generated by each propeller, a term is simply added to account for the additional propellers. Thus, the new acoustic model is

$$L_p = 20 \log_{10} \left(\frac{p^*_{rms}}{p_0} \right) + 10 \log_{10} \left(N \right) , \tag{3.16}$$

in which N is the number of propellers on the aircraft. Simply adding the number of propellers as increased sound intensity reduced the computation time and simplified the observer noise model. Equations (3.15) and (3.16) comprise the Observer Sound Pressure Model.

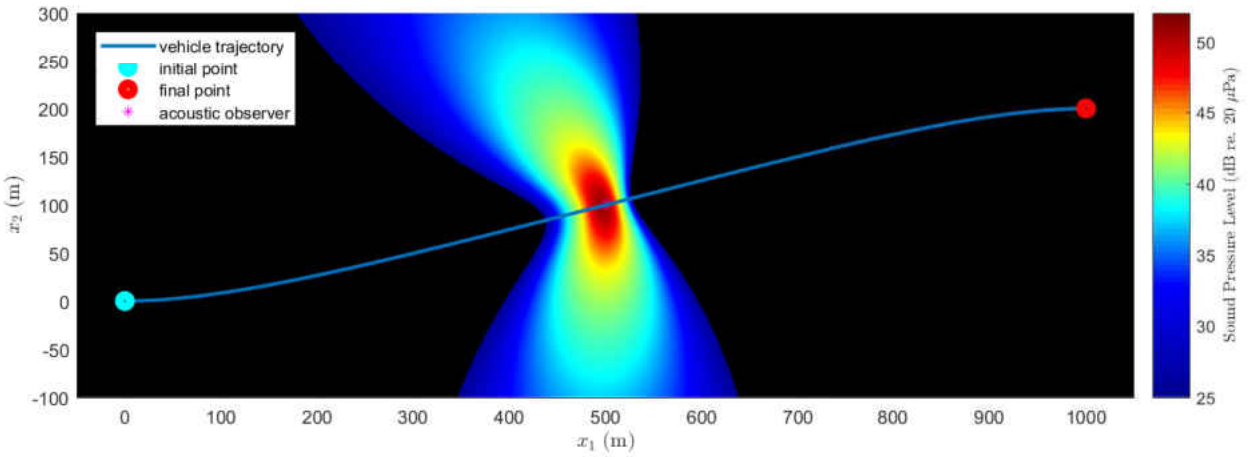

(a) Observer Noise Model with Directivity Considered

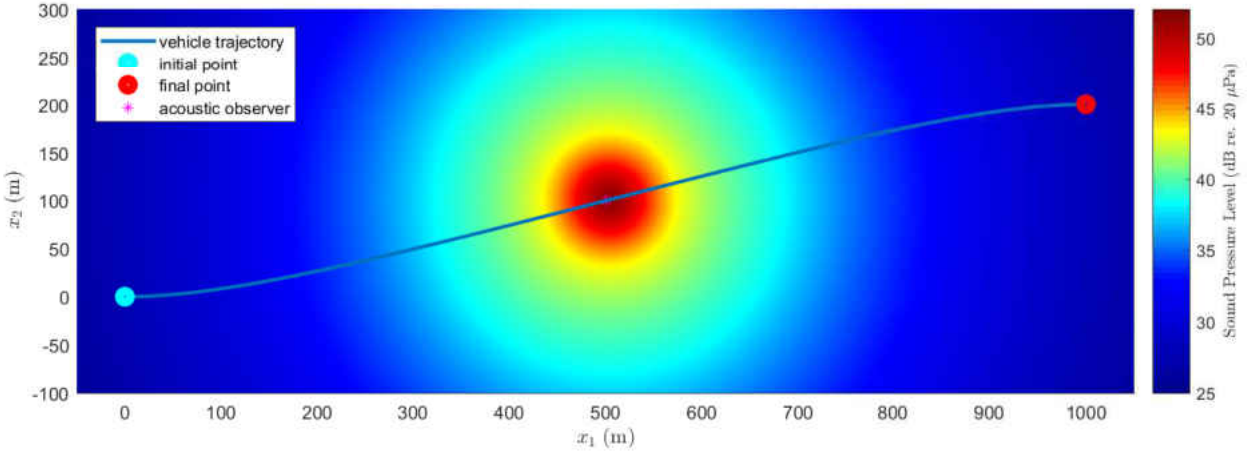

(b) Observer Noise Model with Assumed Uniform Directivity

Figure 3.5 Minimum-Time Trajectory Simulation with the Estimated Noise on the Ground Contour Shown Only at $t = 0.5t_f$

3.3.1 Directivity vs Uniform Directivity Observer Noise Models

Using the propeller noise model developed in §3.3, a simulation was performed to show how the acoustic model operates for a flight path between two points. Figure 3.5 presents a ground contour plane with the estimated SPL at each spatial node at a snapshot in time in the middle of the trajectory when the aircraft is almost directly above the acoustic observer. In Fig. 3.5, variables x_1, x_2 describe respectively the x and y positions. In the first subfigure, the simulation was performed with the acoustic model that considers directivity, Eq. (3.8), and this can be seen in the ground contour plot. Two lobes in which maximum SPL propagates along the ground can be seen at $\pm 108^\circ$ with respect to the forward velocity vector (see Fig. 3.1 in §3.1). In the second subfigure, uniform directivity is assumed in the acoustic model using the SPL at a directivity angle of 108 degrees. One can see the spherical

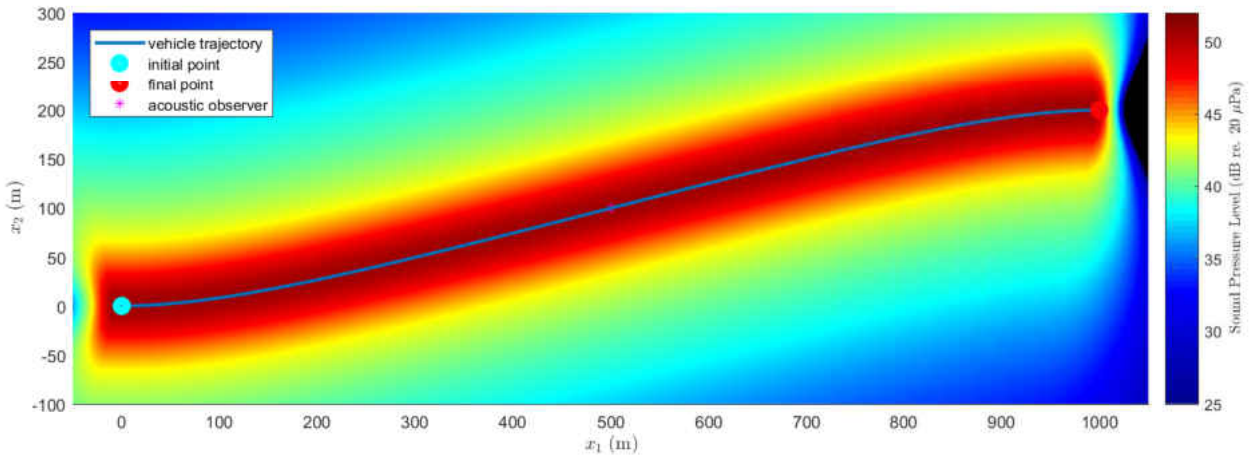

(a) Observer Noise Model with Directivity Considered

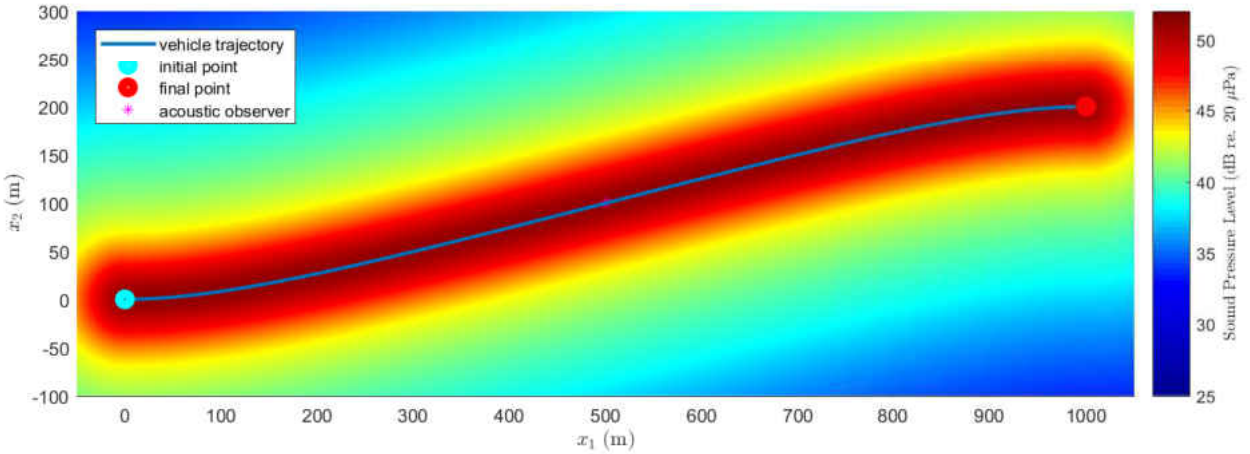

(b) Observer Noise Model with Assumed Uniform Directivity

Figure 3.6 Ground Contour Plot of the Maximum SPL that Each Node Experiences During the Trajectory Simulation

spreading loss that projects radially on the ground contour plot. As this value is the angle of maximum SPL, removal of dependency on ϑ creates a conservative estimate of the SPL at all other angles when compared to the acoustic model with directivity.

The SPL was computed at every ground node at every time step during flight and the maximum SPL that each node was exposed to is shown in Fig. 3.6. In Fig. 3.6a, the acoustic model that considers directivity was used. One can see that the highest SPL occurs directly below the aircraft at each point during the trajectory. The maximum SPL was less than 20 dB near the end of the flight segment at $(x_1, x_2) = (1025, 200)$ m, which is dramatically less than the rest of the ground plane shown, due to the fact that the sound pressure waves do not propagate spherically and this is a minimum SPL angle for the observer noise model.

In Fig. 3.6b, the uniform directivity observer model was used. At the initial and final

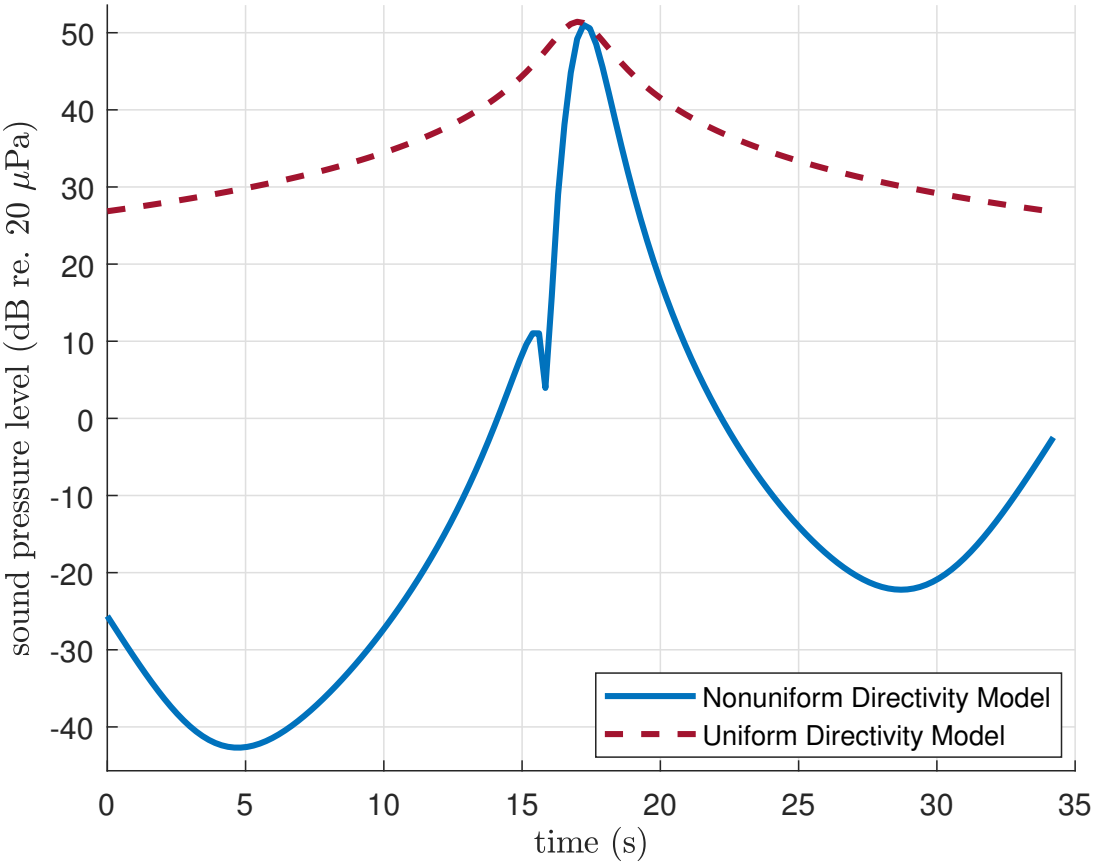

Figure 3.7 Sound Pressure Level vs. Time Shown for the Sound Pressure Model with Uniform and Nonuniform Directivity Considered

points the maximum SPL creates a radial pattern on the ground in contrast with Fig. 3.6a. Note that the maximum SPL contour is relatively the same on the sidelines (near 108°) and thus, there is little difference between the two acoustic models except that there is a computational benefit to using the uniform directivity acoustic model.

For the path optimization approach used here, it is important to determine the maximum SPL at the observer. Figure 3.7 shows the SPL that the observer experienced throughout the simulation using the observer noise model with and without uniform directivity assumed. The maximum observer SPL was 51.01 dB for the nonuniform directivity acoustic model and 51.42 dB for the uniform directivity acoustic model. Note the maximum SPL that the observer experiences is relatively the same for both the nonuniform and uniform simulations. For the current work, the maximum SPL is of primary interest and thus the research will be conducted using the uniform directivity observer noise model as the Observer Sound Pressure Model.

3.4 SUMMARY

In this chapter, two main propeller noise models were developed. The first was the Source Sound Power Model that estimated sound power level, SWL, of the aircraft as a function of vehicle flight parameters. This model will be used in Chapter 4 to develop a control law to modify the vehicle speed as a function of its sound power level. The second model was the Observer Sound Pressure Model that estimated sound pressure level, SPL, at an observer some distance away from the vehicle. This model will be used in Chapter 5 to optimize a trajectory to avoid an acoustically sensitive observer.

CHAPTER 4
SPEED MODIFICATION WITH ACOUSTICS CONSIDERED

In previous chapters, the vehicle system was described and a sound power model was developed to estimate the sound energy emitted by the GL-10 during flight. In this chapter, the sound power model will be incorporated into the vehicle system and an acoustic controller will be developed that will modify the vehicle speed command to the aircraft's flight control system during flight based on the current estimate of sound. This speed modification will be done while the aircraft is flying along a nominal trajectory without perturbation to the flightpath. Figure 4.1 presents a representative trajectory in which horizontal positions x, y, and altitude h are constrained to a rectilinear path from point A to point B and time, t, is a free variable that allows vehicle velocity to be modified during flight.

The objective of this chapter is to demonstrate the feasibility of incorporating an acoustic target into the flight control system of a UAS as a first step toward an acoustically-aware vehicle. Commanded flight speed is changed to reduce the noise generated, thus satisfying a time-varying constraint on sound generated by the vehicle. Figure 4.2 shows a detailed representation of the control architecture used in this study. Specifically, a feedback control system is implemented to modify a nominal velocity command, $v_n(t)$, to the vehicle system based on an acoustic reference, $r(t)$, and a noise metric value, $y_a(t)$. The acoustic reference value is specified a priori, and the noise metric value for the vehicle is estimated using a sound power model. As the figure shows, this approach requires at least two components: (i) a sound power model and (ii) a control law to incorporate the noise metric into the flight control system. The sound power model was described in Chapter 3 and the control law will be developed here. Additionally, the integration of both components into the vehicle system, which includes the flight control system and vehicle dynamics model, will be presented in this chapter.

4.1 BACKGROUND

This work is a first attempt at controlling the acoustics of a vehicle directly through the control system. As a result, an acoustic metric is necessary to estimate the noise generated by the vehicle. This metric can be combined with a new outer loop that is wrapped around the preexisting flight control system to provide an acoustic error for the new acoustic controller to operate on. The velocity command of the vehicle can be modified to increase or decrease the source noise of the vehicle.

As this investigation is done completely in simulation, a preexisting Simulink[35] model

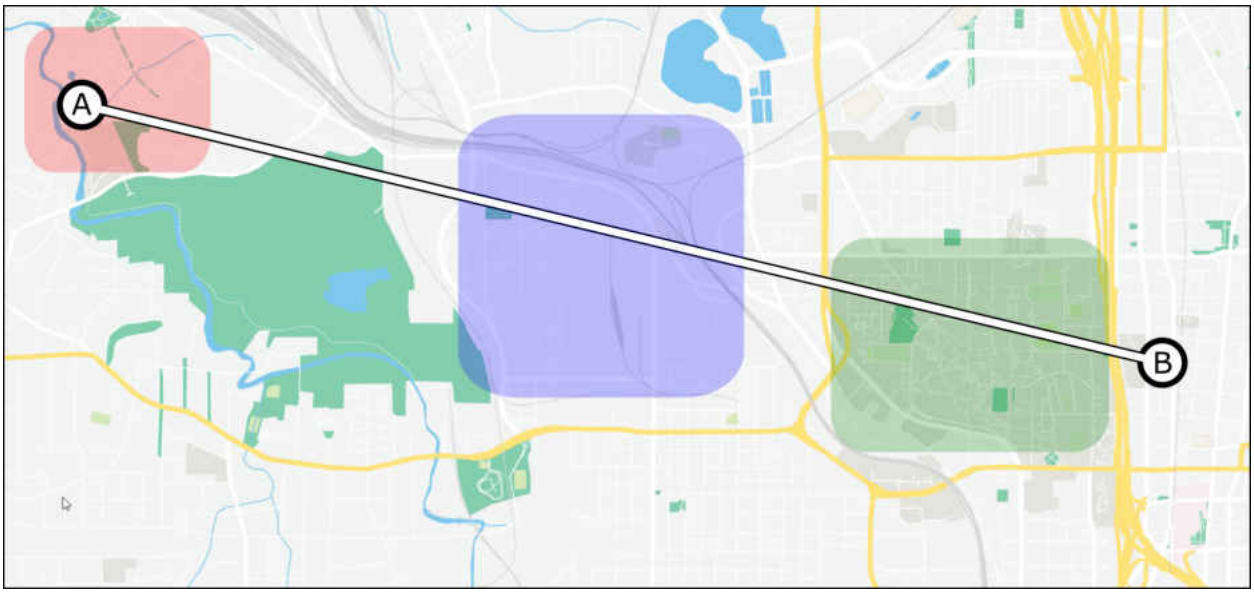

Figure 4.1 Rectilinear Path with Variable Speed over Urban Community

of the vehicle system described in Chapter 2 will be modified. An outer loop is created and wrapped around the vehicle system that will include a new acoustic controller, as shown in Fig. 4.2. This acoustic controller will modify the velocity command based on the acoustic error, $e_a(t)$, and the resulting velocity command is passed through to the vehicle system. The rest of this chapter will describe the specifics of this implementation.

4.2 FLIGHT SPEED MODIFICATION

This section describes the control approach used to integrate an acoustic metric into the flight control system. Discussion of the acoustic controller will include a description of the control law itself, as well as antiwindup functionality that has been implemented.

4.2.1 Proportional-Integral Controller

A detailed block diagram of the control architecture is presented in Fig. 4.2. The control architecture proposed for this project tracks an acoustic reference by modifying the velocity command to the path-following controller. The path-following controller then provides commands to the flight dynamics controller to follow a prescribed path. The acoustic controller uses a PI controller wrapped around the vehicle system as an outer loop. An acoustic target serves as a reference command, $r(t)$, and is determined a priori based on mission defined acoustical constraints. This reference command is filtered using a second-order low pass filter to produce $r_a(t)$, which prevents sharp changes in the command to the

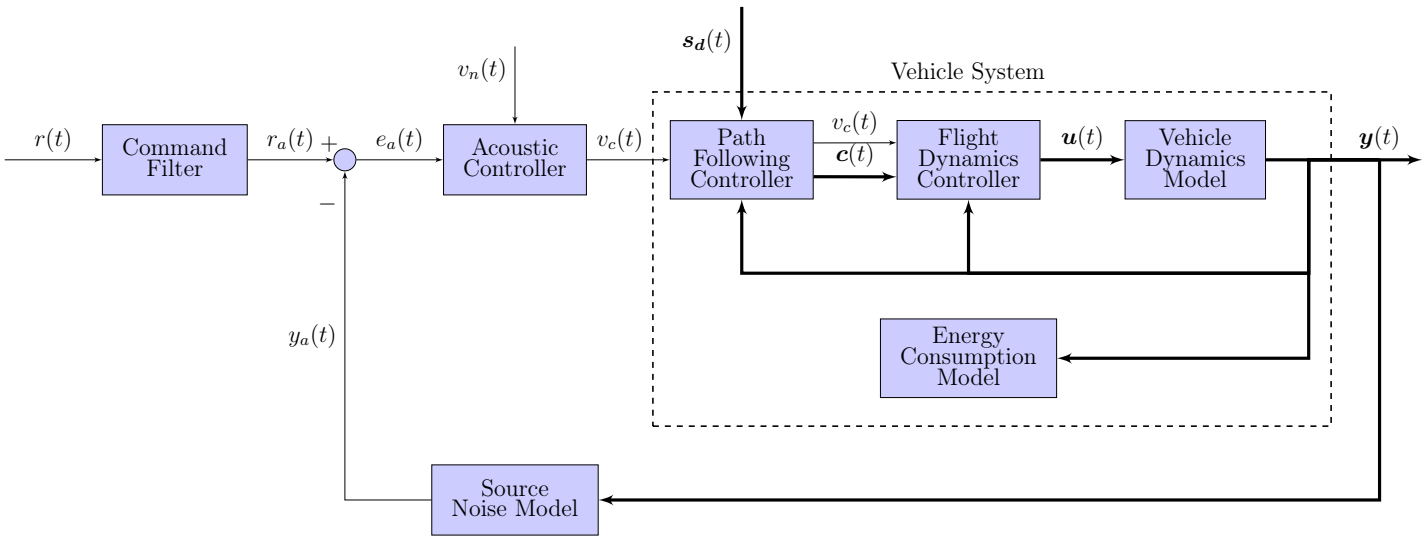

Figure 4.2 Block Diagram of Acoustic Feedback Controller and Vehicle System Model

acoustic controller.

Noise generated by the vehicle is estimated using the source sound power model. Specifically, propeller speed, thrust, and torque of each motor from the system output vector, $\boldsymbol{y}(t)$, are fed into the sound power model to generate a new acoustic estimate, $y_a(t)$, based on the current operating state of the vehicle. The acoustic error, $e_a(t)$, is defined by subtracting the noise estimate from the filtered acoustic reference:

$$e_a\left(t\right) = r_a\left(t\right) - y_a\left(t\right) \ . \tag{4.1}$$

The acoustic controller updates the velocity command to the path-following controller, $v_c(t)$, based on the acoustic error signal. The new commanded velocity is defined as

$$v_c\left(t\right) = v_n\left(t\right) + \Delta v_a\left(t\right) \ , \tag{4.2}$$

in which $v_n(t)$ is the nominal velocity command, and $\Delta v_a\left(t\right)$ is generated using the PI controller presented in Eq. (4.3), assuming no saturation,

$$\Delta v_a\left(t\right) = K_p e_a\left(t\right) + K_i \int_0^t e_a\left(\tau\right) d\tau \ , \tag{4.3}$$

in which K_p and K_i are tuneable gains of the PI controller. Integral control was added to reduce the steady state error to zero. Derivative control, commonly used in this class of controllers, provided no benefit and was not used in this control law. Combining Eqs.

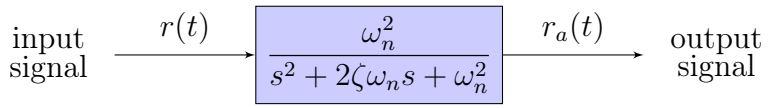

Figure 4.3 Block Diagram of the Command Filter

(4.2) and (4.3) produces Eq. (4.4), defining the relationship between the acoustic error, the nominal velocity command, and the modified velocity command, given as

$$v_c\left(t\right) = v_n\left(t\right) + \left[K_p e_a\left(t\right) + K_i \int_0^t e_a\left(\tau\right) d\tau\right] \tag{4.4}$$

The updated speed command will increase or decrease the vehicle's velocity through higher or lower motor speeds, thereby increasing or reducing the vehicle noise, $y_a(t)$. By analyzing vehicle dynamics and acoustic response during simulations, appropriate gains were tuned to $K_p = 3\ m/s \cdot dB^{-1}$ and $K_i = 1\ m/s^2 \cdot dB^{-1}$.

4.2.2 Command Filter

As the aircraft enters or exits an acoustically sensitive region (such as the red, blue, and green regions shown in Fig. 4.1), a step change in the acoustic target occurs. The resulting step change in the acoustic error can result in an excessively large velocity command to the flight control system that is not physically possible for the vehicle to follow.[68] A second-order filter is used to slow the acoustic reference rate of change to prevent a sharp change in input to the acoustic controller (see Fig. 4.2). Parameters are selected to prevent the acoustic controller from commanding a response significantly quicker than the vehicle system can follow. A block diagram of the second-order command filter is shown in Fig. 4.3.

To develop an appropriate filter, it is necessary to determine the natural frequency of the system. The time constant of the nominal closed-loop response, without acoustic control, can be calculated by simulating the settling time of the vehicle system to a step input. Assuming that the response settles to within 2 percent of the steady state value and the system exhibits second-order behavior, the relationship between settling time and the time constant is[69]

$$e^{-t_s/\tau_s} = 0.02\ . \tag{4.5}$$

Solving for the second-order time constant, τ_s, results in

$$\tau_s \approx \frac{t_s}{3.912}\ . \tag{4.6}$$

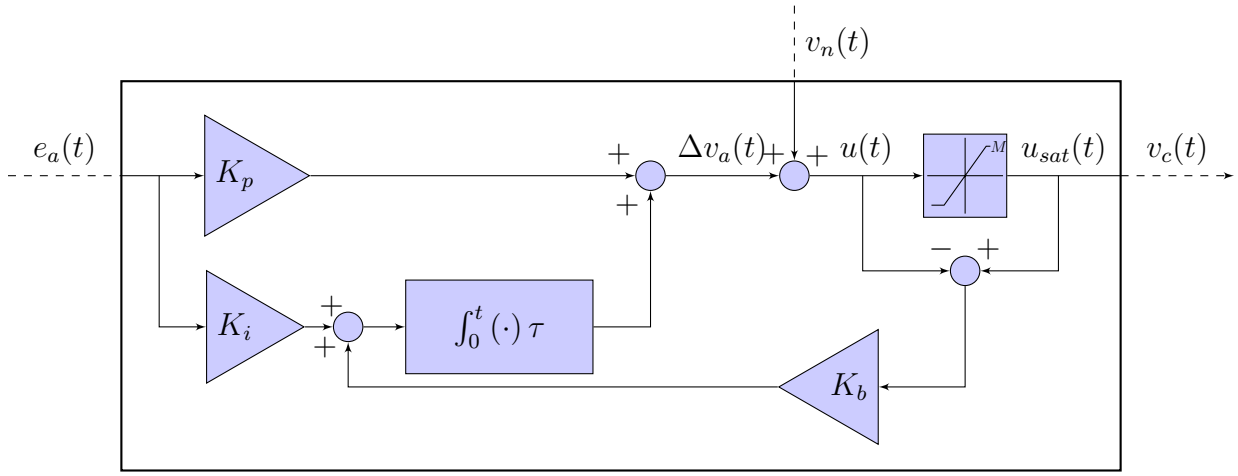

Figure 4.4 Detailed Block Diagram of Acoustic Controller with Antiwindup

A simulation was performed to observe the settling time to a velocity command step response of the vehicle system. The settling time of the velocity response was estimated to be 7.7 seconds, and using Eq. (4.6), the time constant of the system was calculated as 1.9 seconds. The time constant, τ_s, is inversely proportional to the damping ratio, ζ, and the natural frequency, ω_n, (assuming second-order behavior), shown by[70]

$$\tau_s = \frac{1}{\zeta \omega_n} \, . \tag{4.7}$$

Zero overshoot between the reference signal and filtered reference signal is desired, and thus, a critically damped case in which $\zeta = 1$ will be considered for the transfer function of the command filter. Equation (4.7) can be used to calculate the natural frequency as 3.2 rad/s. Utilizing a second-order filter, the transfer function of the command filter is thus

$$H\,(s) = \frac{10.32}{s^2 + 6.426s + 10.32} \, . \tag{4.8}$$

This filter was implemented in Simulink[35] using an initial output transfer function block where the initial output is equivalent to the initial acoustic target when the acoustic controller is enabled.

4.2.3 Antiwindup Logic

Although a filter was designed to condition the acoustic reference to prevent unrealistic commands to the flight control system, it is still necessary to implement integrator antiwindup logic in the acoustic controller. One possible deficiency in the system design is

that the acoustic controller may try to force the vehicle outside of the flight envelope during a mission as the aircraft operates with time-varying acoustic targets. In this case, error accumulated while the vehicle speed is capped by the flight control system will result in a longer response time once the vehicle returns to a state in which the acoustic controller can function properly. This antiwindup logic will aide in maintaining stable flight throughout the mission by avoiding high gain commands that result in overshooting desired flight attitudes. Additionally, it will reduce the response time due to integral error once the aircraft returns from an acoustic target outside of its operational capacity.

As shown in Fig. 4.4, the control signal, $u(t)$, is saturated to create $u_{sat}(t)$. Saturating the control input additionally protects the flight control system from a high amplitude velocity command in the event that the command filtering is not sufficient. The logic in the saturation block in Fig. 4.4 is defined as

$$u_{sat}(t) = \begin{cases} M_{\max} & u(t) > M_{\max} \\ u(t) & M_{\max} \geq u(t) \geq M_{\min} \\ M_{\min} & M_{\min} > u(t) \end{cases}, \tag{4.9}$$

in which $M_{\max} = 31$ m/s, just below the the maximum flight speed of the GL-10, and $M_{\min} = 19$ m/s, just above the stall speed of the vehicle. The difference between the control signal and the saturated control signal (i.e., the saturation error) is multiplied by a gain, K_b, and subsequently fed back into the integral path of the PI controller. Incorporating antiwindup into Eq. (4.4) results in the following control law

$$v_c(t) = v_n(t) + \left[K_p e_a(t) + \int_0^t K_i e_a(\tau) + K_b \left\{ u_{sat}(\tau) - u(\tau) \right\} d\tau \right] \tag{4.10}$$

The antiwindup gain affects how quickly the integral term is reset to avoid accumulating excessive error. By running simulations and observing how quickly the unsaturated velocity command, $u(t)$, leveled out, the saturation error gain was tuned to $K_b = 100$ s^{-1}.

4.3 SIMULATION RESULTS

Simulations were performed to evaluate the performance of the acoustic controller and the antiwindup logic. This section will begin with discussion of a simulated flight mission operating with and without the acoustic controller enabled. Then, a discussion of data collected to validate the antiwindup logic will follow. Lastly, results of the energy consumption model will be discussed to compare energy usage with and without the acoustic controller enabled.

4.3.1 Acoustic Controller Performance

To evaluate the performance of the acoustic controller, a simulation was performed that encompassed low, medium, and high acoustic targets. These acoustic targets could be appropriate for residential, commercial, and agricultural zones, each of which might have a different sensitivity to a noise source. The low, medium, and high acoustic targets were respectively 121, 125, and 129 dB (referenced to W_0) SWL. An important point to stress is the acoustic metric is based on source noise power, and not sound pressure at an observer. These target sound power levels were arbitrarily chosen to demonstrate the concept in this initial study. For all simulations, the nominal mission trajectory is SLUF (i.e., constant velocity).

Figure 4.5 presents results of a flight simulation of the GL-10 operating under acoustic control. The simulation was started at $t = -20$ seconds to allow the aircraft simulation to reach a trimmed state and SLUF before the acoustic controller was enabled at $t = 0$ seconds. The desired altitude was specified as 30.5 m. Once the acoustic controller was enabled, a medium acoustic target was set, followed by a low acoustic target, and ending with a high acoustic target. This arrangement demonstrated the concept of a vehicle operating through regions with varying noise constraints.

As shown in Fig. 4.5a, the system tracked the acoustic command very well, converging to the value within 5 seconds or less for each acoustic command change. At approximately 46 seconds, the acoustic controller had a 1% overshoot, which was acceptable for the purposes of this study.

Figure 4.5b presents the velocity and altitude of the aircraft during the simulation. The nominal velocity command, $v_n(t)$, was a constant 28 m/s, indicated by the dashed black line. Once the acoustic controller was enabled, it reduced the commanded velocity from 28 to approximately 26 m/s. Some overshoot occurs in the velocity command, as seen at 0, 20, and 40 seconds, but overshoot is less in the vehicle noise and velocity responses. The change in velocity command resulted in some error in altitude tracking due to the phugoid mode of the aircraft dynamics. However, the deviation was small enough to be of no concern.

4.3.2 Antiwindup Logic Validation

Two simulations of the mission described in §4.3.1, without and with antiwindup enabled, were performed to validate this feature. In the first simulation without antiwindup logic, an acoustic reference value larger than the sound power level the vehicle could produce was sent to the acoustic controller, which commanded a velocity above the saturation limit of 31 m/s, shown in solid green in Fig. 4.6a. This large input resulted in a steady state error,

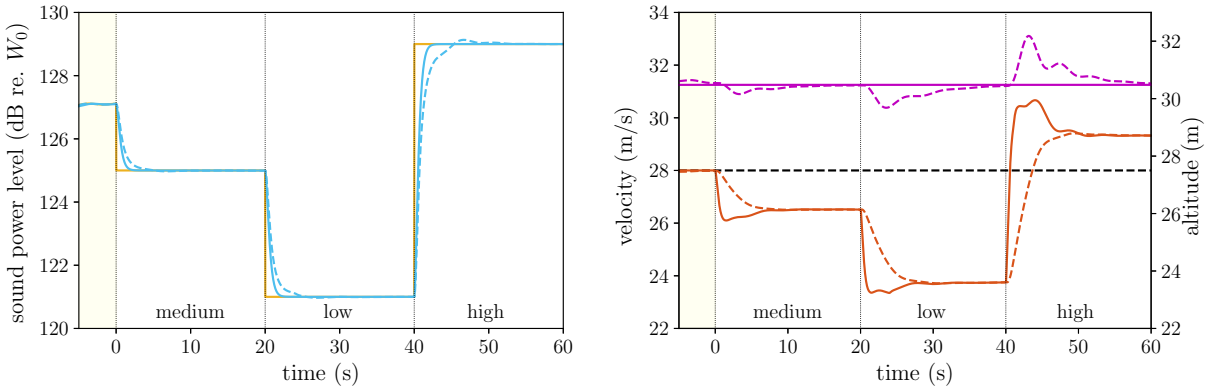

(a) Sound power level vs. time; acoustic target (—), command (—), and acoustic state (----)

(b) Velocity and altitude vs. time; nominal command (----), controller command (—), and vehicle velocity (----); altitude command (—) and vehicle altitude (----)

Figure 4.5 Flight Simulations with Acoustic Control Enabled

shown in Fig. 4.6b, in which the proportional term (shown in solid light blue) converged to approximately 10 m/s and the integral term (shown in solid red) increased without bound.

A second flight simulation was performed, and with antiwindup enabled, there are differences in the proportional and integral term behavior. The proportional term initially becomes larger than the term without antiwindup enabled due to the initial steady state error, however, the integral term decreases to cancel the proportional term, driving the saturation error to zero. This behavior is illustrated in Fig. 4.6a as the unsaturated velocity command, shown in orange red with stars, converges to the saturated velocity command of 31 m/s.

4.3.3 Energy Consumption Model

Operating under acoustic control is expected to affect the energy consumed, and the following simulations were performed to investigate the tradeoffs between acoustically-aware and nominal flight. The first flight simulation was the same as the one shown in Fig. 4.5 and the second was a nominal SLUF mission without acoustic control.

A necessary task is to compare data over equal distances because one simulation resulted in a further distance traveled. The limiting case was the simulation with acoustic control enabled, in which the total distance traveled during the 60 second mission was 1589 m. For this case, over the 1589 m traveled, the GL-10 motors used 1156 kJ of energy. With acoustic control off, the GL-10 consumed 1235 kJ to travel the same 1589 m as the sim-

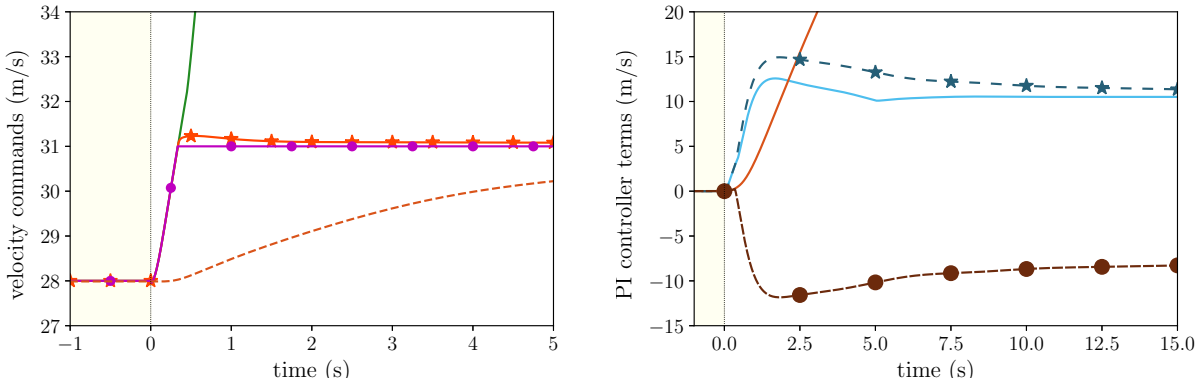

(a) Velocity commands vs. time; unsaturated velocity command without antiwindup enabled (——), unsaturated velocity command with antiwindup (—★—), saturated velocity command (—●—), and vehicle velocity with antiwindup enabled (----)

(b) PI controller terms vs. time; proportional term (——) and integral term (——) without antiwindup logic enabled; proportional term (-★-) and integral term (-●-) with antiwindup logic enabled

Figure 4.6 Flight Simulations with and without Antiwindup Engaged

ulation with acoustic control enabled. Therefore, with the acoustic controller enabled, the GL-10 took 5.7% more time to reach a target distance of 1589 m, while consuming 6.4% less energy. This result may be intuitive, as motors running at a slower speed consume less energy, but nonetheless, the model provides the capability for energy consumption analysis in future missions in which the results may not be so apparent.

4.4 LIMITATIONS

The method described in this chapter demonstrates the capability of interfacing with a preexisting flight control system to modify the acoustics of a vehicle, but the method is not without limitations. For one, the method developed here modifies the velocity command input to the flight control system. Thus, for the method described in this chapter to work, the flight control system needs to accept a velocity command input. As a result, it may be difficult or impossible to interface with any flight control system different in structure from the one described in this chapter. The Source Sound Power Model developed is based on loading noise only, without consideration for thickness noise and there are many limitations described in literature for Gutin's method. Specifically, Gutin does not account for unsteady inflow, forward flight speed, angle of attack, or broadband noise. Lastly, this work was performed in simulation only without experimental validation.

4.5 SUMMARY

The purpose of this work was to create an acoustic controller and to demonstrate its use for modifying the commanded velocity of an aircraft based on time-varying acoustic targets. A PI acoustic controller was designed and implemented. Antiwindup functionality was implemented to prevent excessive error accumulation in the integrator term in the presence of command saturation. An energy consumption model was developed to allow for analysis of energy used during missions. Simulations were performed to investigate the efficacy of the proposed acoustic controller and antiwindup logic. Simulation results show that the acoustic controller tracks a total radiated sound power target well, adjusting vehicle speed to converge to the target level within 7 to 10 seconds. Antiwindup logic was able to prevent the controller from accumulating excess error. The energy consumption model showed that, for this specific mission, the GL-10 used less energy under acoustic control. While there are limitations to consider, this work resulted in a flight control system that provided automatic management of the sound generated during flight, demonstrating the capability of using sound as a potential performance metric for consideration during mission planning.

CHAPTER 5
PATH PLANNING WITH ACOUSTICS CONSIDERED

In this chapter, an optimization of the trajectory will be performed to spatially avoid an acoustically sensitive observer while satisfying initial and final boundary conditions with an optimal specified-time and minimum control effort solution. Since the sound pressure decays with distance from a source, modifying the trajectory to avoid an observer will reduce the noise experienced by the observer.

The chapter begins with an overview of the method used to optimize an aircraft trajectory in §5.1. Then, the equations of motion and costate equations for optimality will be derived in §5.2. An acoustic constraint will be implemented by incorporating the Observer Sound Pressure Model developed in Chapter 3 into the optimization algorithm; this process will be described in §5.3. Simulation results will be presented in §5.4, limitations of the method proposed will be described in §5.5, followed by a summary of the work performed in §5.6.

5.1 BACKGROUND

In this work, a flight segment will be analyzed and modified over an acoustically sensitive area; examples of such areas are shaded in Fig. 5.1. Within this acoustically sensitive area exists an acoustic observer. The figure presents a curvilinear path from location A to location B which is flown with constant velocity and avoids direct overflight of the acoustic observer, and achieves certain departure and arrival conditions at points A and B.

An algorithm determines the acceptable trajectory from points A to B in a specified amount of time. This algorithm contains an optimization routine to create the trajectory and logic to modify the specified flight time, as shown in Fig. 5.2. If the flight time is greater than the straight-line required flight time (which it will be due to the nearby acoustic observer), then the trajectory will be curved. As the flight time increases, the trajectory becomes more curved; this curved flight path is what provides the capability to avoid a noise sensitive area.

To modify and optimize the trajectory, functional optimization will be employed to minimize control effort subject to a flight time constraint. Functional optimization is a solution method that involves identifying unknown functions of time that will minimize a performance index.[40] In the trajectory optimization problem, the performance index will be the integrated control effort of the aircraft, which also minimizes the curvature[1] of the

[1]The curvature is the deviation from a straight line.

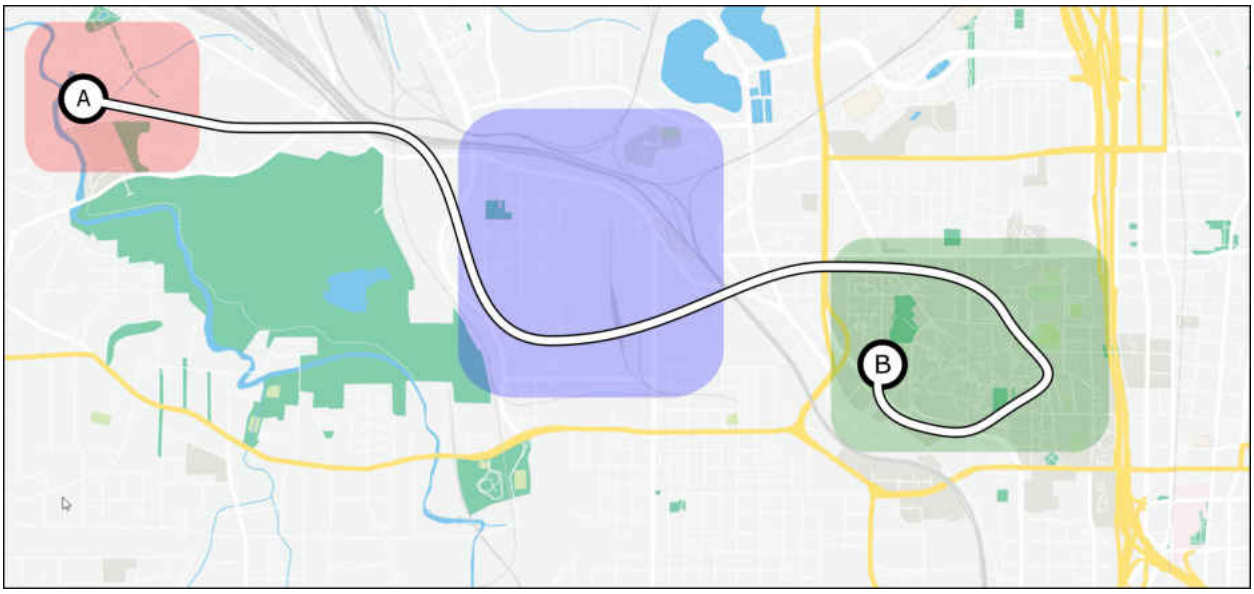

Figure 5.1 Curvilinear Path with Constant Speed over Urban Community

flight path. Optimization of the performance index provides a direct process to achieve small control effort.

The SPL at the observer during the trajectory is then calculated as a function of time based on the velocity of the aircraft and distance from the observer using the Observer Sound Pressure Model developed in Chapter 3. If the maximum SPL of this time series vector violates a maximum SPL threshold, the flight duration is increased to provide the optimization routine additional time to expand the flight trajectory while minimizing control effort at a constant flight speed. If the maximum SPL of this time series is less than the SPL threshold, the flight duration is decreased and the process is repeated. This process is described by the yellow decision tree blocks in Fig. 5.2. The time input to the optimization routine is modified by this decision tree process. Once the SPL constraint is met, the algorithm ends, as shown by the "stop algorithm" block in Fig. 5.2, and the algorithm output is the minimum-time flight trajectory that also satisfies the desired SPL at an observer.

5.2 OPTIMAL TRAJECTORY DEVELOPMENT

To determine an optimal trajectory, equations for optimality are necessary. These dynamic equations are called the state and costate (or adjoint) equations, and have been previously derived in the literature for a one-dimensional case.[71] In this section, equations for optimality for a two-dimensional double integrator plant will be presented, which, when combined with a shooting method to determine the appropriate initial conditions, will be used to calculate the optimal trajectory.

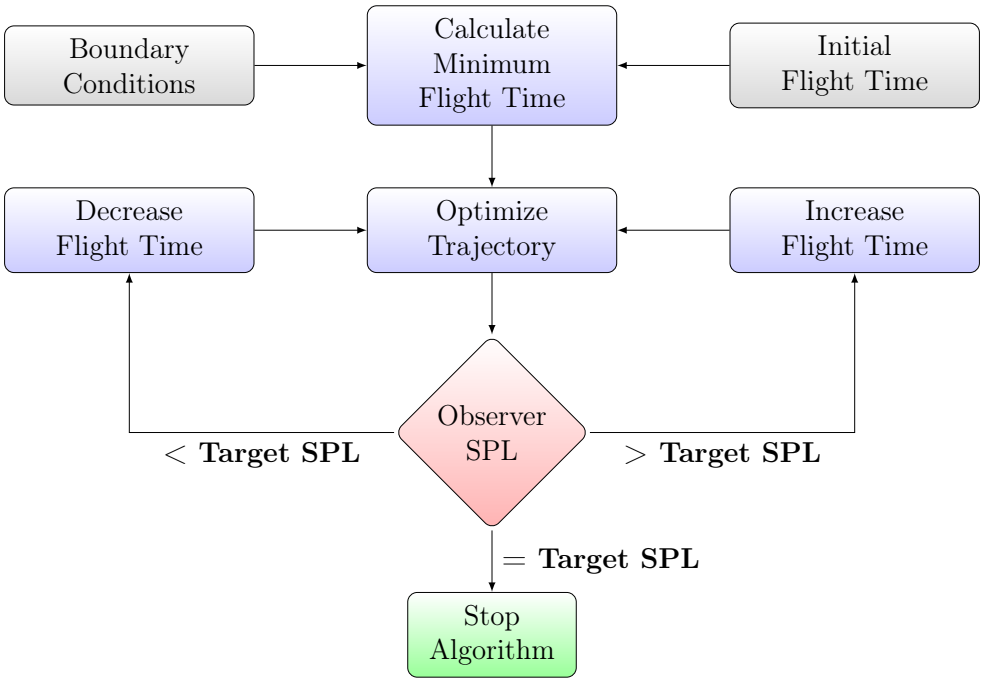

Figure 5.2 Path Planning Flow Chart.

For this work, the aircraft is modeled as a point mass moving through space to simplify the equations of motion. With a control objective to fly the acoustically sensitive trajectory at a specified constant speed, an equality constraint on the flight speed of the aircraft will be imposed and incorporated in the dynamic equations. This imposed equality indirectly constrains the acceleration of the vehicle, since it restricts the two individual velocity states to a constant velocity magnitude. Without this constraint, the two states will not be tied together and this can lead to the creation of unrealistic trajectories that violate the capabilities of the aircraft. Additional position and velocity states are altitude and change in altitude, but these are fixed and are not part of the derivation of the optimal equations.

5.2.1 Dynamic System

As the altitude is assumed constant, the vehicle position is described by horizontal coordinates x and y. The vehicle state can be represented by

$$\boldsymbol{x} = [\, x(t)\ y(t)\ \dot{x}(t)\ \dot{y}(t)\,]^T = [\, x_1\ x_2\ x_3\ x_4\,]^T, \tag{5.1}$$

in which $\boldsymbol{x} \in \mathbb{R}^4$ is a state vector, (x_1, x_2) are the vehicle positions and (x_3, x_4) are the flight velocities. The control vector input to the system, $\boldsymbol{u} \in \mathbb{R}^2$, can be represented by the

acceleration of the vehicle as

$$\boldsymbol{u} = [\, \ddot{x}(t)\ \ddot{y}(t)\,]^T = [\, u_1\ u_2\,]^T. \tag{5.2}$$

The system dynamics are described by the following linear differential equations

$$\dot{\boldsymbol{x}} = \boldsymbol{f}(\boldsymbol{x}, \boldsymbol{u}, t)\,, \tag{5.3}$$

for time period $t_0 \leq t \leq t_f$, in which

$$\boldsymbol{f}(\boldsymbol{x}, \boldsymbol{u}, t) = A\boldsymbol{x} + B\boldsymbol{u} = \begin{bmatrix} 0 & 0 & 1 & 0 \\ 0 & 0 & 0 & 1 \\ 0 & 0 & 0 & 0 \\ 0 & 0 & 0 & 0 \end{bmatrix} \begin{bmatrix} x_1 \\ x_2 \\ x_3 \\ x_4 \end{bmatrix} + \begin{bmatrix} 0 & 0 \\ 0 & 0 \\ 1 & 0 \\ 0 & 1 \end{bmatrix} \begin{bmatrix} u_1 \\ u_2 \end{bmatrix}\,. \tag{5.4}$$

The system is subject to the following boundary conditions and constraints

$$\boldsymbol{x}_0 = \boldsymbol{x}(t_0), \tag{5.5}$$

$$\boldsymbol{x}_f = \boldsymbol{x}(t_f), \tag{5.6}$$

$$x_3{}^2 + x_4{}^2 = \nu^2, \tag{5.7}$$

in which $\boldsymbol{x}_0 = \boldsymbol{x}(t_0)$ is the initial state at t_0, $\boldsymbol{x}_f = \boldsymbol{x}(t_f)$ is the final state at a specified final time, t_f, and ν is the constrained flight speed, which is also specified.

5.2.2 Performance Index

To create an optimal trajectory, it is desired to find the input functions $\boldsymbol{u}$ that minimize a performance index of the form

$$J = \int_{t_0}^{t_f} L(\boldsymbol{x}, \boldsymbol{u}, t)dt\,, \tag{5.8}$$

in which J is the scalar performance index from initial to final time and L is the Lagrangian subject to the boundary conditions and state constraints of the system. The desired objective is to minimize the control effort of the aircraft when flying between prescribed initial and final conditions, subject to the velocity constraint, which means the Lagrangian of this system is

$$L = \frac{1}{2}\boldsymbol{u}^T\boldsymbol{u}\,. \tag{5.9}$$

The Hamiltonian, a scalar value, is defined as

$$H(\boldsymbol{x}, \boldsymbol{u}, \boldsymbol{\lambda}, t) = L(\boldsymbol{x}, \boldsymbol{u}, t) + \boldsymbol{\lambda}^T \boldsymbol{f}(\boldsymbol{x}, \boldsymbol{u}, t) \ , \tag{5.10}$$

in which $\boldsymbol{\lambda} \in \mathbb{R}^4$ is the Lagrangian multiplier vector and is defined as

$$\boldsymbol{\lambda} = [\, \lambda_1(t) \ \lambda_2(t) \ \lambda_3(t) \ \lambda_4(t) \,]^T, \tag{5.11}$$

in which the Lagrangian multipliers are functions of time and are (λ_1, λ_2) for position and (λ_3, λ_4) for velocity.

5.2.3 Equality Constraint on State Variables

As the dynamic constraint equations were adjoined to the performance index argument with Lagrangian multiplier functions to form the Hamiltonian in Eq. (5.10), a constraint on the control and state variables will be adjoined to the original Hamiltonian using a constraint multiplier function to form the following augmented Hamiltonian scalar

$$H(\boldsymbol{x}, \boldsymbol{u}, \boldsymbol{\lambda}, t) = L(\boldsymbol{x}, \boldsymbol{u}, t) + \boldsymbol{\lambda}^T \boldsymbol{f}(\boldsymbol{x}, \boldsymbol{u}, t) + \mu C(\boldsymbol{x}, \boldsymbol{u}, t) \, , \tag{5.12}$$

in which μ is the constraint multiplier function, performing the same purpose as the Lagrangian multipliers, and C is the constraint function on the control and state variables. In this problem, only a constraint on the state variables exists, which, from Eq. (5.7), is given by

$$S(\boldsymbol{x}, t) = 0 = \frac{1}{2} \left\{ {x_3}^2 + {x_4}^2 - \nu^2 \right\} \ , \tag{5.13}$$

in which ν is the flight velocity constraint of 30 m/s. The constraint function does not have an explicit dependence on the control variables, but rather an implicit dependence given by

$$\begin{bmatrix} \dot{x}_3 \\ \dot{x}_4 \end{bmatrix} = \begin{bmatrix} 1 & 0 \\ 0 & 1 \end{bmatrix} \begin{bmatrix} u_1 \\ u_2 \end{bmatrix} \ . \tag{5.14}$$

To form a constraint equation that has an explicit dependence on the control variables, the time derivative along the path can be taken. As long as this time derivative is zero, this constraint function is appropriate for the duration of the flight segment, $t_0 \leq t \leq t_f$. This artificial construction of constraint C can be demonstrated by the following derivation:

$$\frac{dS}{dt} = 0 = \frac{\partial S}{\partial t} + \frac{\partial S}{\partial \boldsymbol{x}} \dot{\boldsymbol{x}} \, , \tag{5.15}$$

$$C(\boldsymbol{x},\boldsymbol{u},t) = 0 = \frac{\partial S}{\partial t} + \frac{\partial S}{\partial \boldsymbol{x}}^T \boldsymbol{f}\left(\boldsymbol{x},\boldsymbol{u},t\right) . \tag{5.16}$$

In Eq. (5.16), constraint C is chosen as dS/dt which introduces $\boldsymbol{u}$ through function f. If the first differentiation does not result in a constraint function with an explicit dependence on the control variables, then the process is repeated until it does.[40]

Performing the derivation results in

$$0 = \frac{\partial}{\partial t}\left(x_3^2 + x_4^2 - \nu^2\right) + \begin{bmatrix} \frac{\partial}{\partial x_1}\left(x_3^2 + x_4^2 - \nu^2\right) \\ \frac{\partial}{\partial x_2}\left(x_3^2 + x_4^2 - \nu^2\right) \\ \frac{\partial}{\partial x_3}\left(x_3^2 + x_4^2 - \nu^2\right) \\ \frac{\partial}{\partial x_4}\left(x_3^2 + x_4^2 - \nu^2\right) \end{bmatrix}^T \left(\begin{bmatrix} 0 & 0 & 1 & 0 \\ 0 & 0 & 0 & 1 \\ 0 & 0 & 0 & 0 \\ 0 & 0 & 0 & 0 \end{bmatrix} \begin{bmatrix} x_1 \\ x_2 \\ x_3 \\ x_4 \end{bmatrix} + \begin{bmatrix} 0 & 0 \\ 0 & 0 \\ 1 & 0 \\ 0 & 1 \end{bmatrix} \begin{bmatrix} u_1 \\ u_2 \end{bmatrix} \right) , \tag{5.17}$$

$$0 = 2x_3\dot{x}_3 + 2x_4\dot{x}_4 + \begin{bmatrix} 0 & 0 & 2x_3 & 2x_4 \end{bmatrix} \begin{bmatrix} x_3 \\ x_4 \\ u_1 \\ u_2 \end{bmatrix} , \tag{5.18}$$

$$0 = 2x_3\dot{x}_3 + 2x_4\dot{x}_4 + 2x_3u_1 + 2x_4u_2 , \tag{5.19}$$

$$0 = \frac{1}{2}x_3\left(\dot{x}_3 + u_1\right) + \frac{1}{2}x_4\left(\dot{x}_4 + u_2\right) . \tag{5.20}$$

As Eq. (5.20) has an explicit dependence on $\boldsymbol{u}$, it will act as a constraint on the control variable so long as $C_{\boldsymbol{u}}$ is nonzero for any given $\boldsymbol{u}$.[2] To illustrate the nature of the constraint in Eq. (5.20), solving for x_4 by rearranging Eq. (5.20) yields the expression:

$$x_4 = \frac{x_3(\dot{x}_3 + u_1)}{\dot{x}_4 + u_2} . \tag{5.21}$$

This relationship ties the constraint to the input and shows that state x_4 is dependent on x_3 and higher derivatives of x_3 and x_4. Note Eq. (5.21) does not contain the actual constraint, that the velocity must be 30 m/s, but rather enforces a constant velocity magnitude. The fixed speed condition must be incorporated into the simulation by adding

$$S(\boldsymbol{x},t) = 0 \tag{5.22}$$

as a boundary condition at t_0, i.e.,

$$x_3(t_0)^2 + x_4(t_0)^2 = \nu^2 , \tag{5.23}$$

which will be dependent on the desired initial heading angle. Additionally, a final boundary

[2] §3.3 of Bryson and Ho.[40]

condition will be imposed of the form

$$x_3(t_f)^2 + x_4(t_f)^2 = \nu^2 \, . \tag{5.24}$$

Adding the initial condition given by Eq. (5.23), coupled with the state constraint in Eq. (5.21), ensures that the velocity will be constrained to ν throughout the generated trajectory.

5.2.4 Euler-Lagrange Equations and Equations for Optimality

From the previous relations, the Euler-Lagrange equations can be defined as

$$\dot{\boldsymbol{\lambda}}^T = -\frac{\partial H}{\partial \boldsymbol{x}} \, , \tag{5.25}$$

along with the augmented Hamiltonian condition,

$$\frac{\partial H}{\partial \boldsymbol{u}}^T \equiv 0 = \mathcal{L}_{\boldsymbol{u}}{}^T + \boldsymbol{f}_{\boldsymbol{u}}{}^T \boldsymbol{\lambda} + C_{\boldsymbol{u}}{}^T \mu \, . \tag{5.26}$$

It is necessary to substitute u_1, u_2 for $\dot{x}_3$, $\dot{x}_4$ respectively, in Eq. (5.20), or

$$C(\boldsymbol{x}, \boldsymbol{u}, t) = 0 = \frac{1}{2} x_3 (2u_1) + \frac{1}{2} x_4 (2u_2) \, , \tag{5.27}$$

$$C(\boldsymbol{x}, \boldsymbol{u}, t) = 0 = x_3 u_1 + x_4 u_2 \, . \tag{5.28}$$

Performing the derivation below yields the following relationships for the Eq. (5.26) optimality condition.

$$0 = \begin{bmatrix} u_1 \\ u_2 \end{bmatrix} + \begin{bmatrix} 0 & 0 & 1 & 0 \\ 0 & 0 & 0 & 1 \end{bmatrix} \begin{bmatrix} \lambda_1 \\ \lambda_2 \\ \lambda_3 \\ \lambda_4 \end{bmatrix} + C_{\boldsymbol{u}}{}^T \mu \, , \tag{5.29}$$

$$0 = \begin{bmatrix} u_1 \\ u_2 \end{bmatrix} + \begin{bmatrix} 0 & 0 & 1 & 0 \\ 0 & 0 & 0 & 1 \end{bmatrix} \begin{bmatrix} \lambda_1 \\ \lambda_2 \\ \lambda_3 \\ \lambda_4 \end{bmatrix} + \frac{\partial}{\partial \boldsymbol{u}}^T \left[\frac{\partial S}{\partial t} + \frac{\partial S}{\partial x}^T f(\boldsymbol{x}, \boldsymbol{u}, t) \right] \mu, \tag{5.30}$$

$$0 = \begin{bmatrix} u_1 \\ u_2 \end{bmatrix} + \begin{bmatrix} 0 & 0 & 1 & 0 \\ 0 & 0 & 0 & 1 \end{bmatrix} \begin{bmatrix} \lambda_1 \\ \lambda_2 \\ \lambda_3 \\ \lambda_4 \end{bmatrix} + \frac{\partial}{\partial \boldsymbol{u}}^T \left[x_3 u_1 + x_4 u_2 \right] \mu \, , \tag{5.31}$$

$$0 = \begin{bmatrix} u_1 \\ u_2 \end{bmatrix} + \begin{bmatrix} \lambda_3 \\ \lambda_4 \end{bmatrix} + \begin{bmatrix} x_3 \\ x_4 \end{bmatrix} \mu \, . \tag{5.32}$$

Thus, with a rearrangement, Eq. (5.32) results in the following two relationships

$$u_1 = \dot{x}_3 = -\lambda_3 - x_3 \mu \, , \tag{5.33}$$

$$u_2 = \dot{x}_4 = -\lambda_4 - x_4\mu\,. \tag{5.34}$$

The constraint multiplier function, μ, binds the two velocity states together to form the velocity constraint equation. Equations (5.28), (5.33), and (5.34) result in a system of three equations and three unknowns that can be used to solve for the control inputs, u_1 and u_2 as functions of the states and Lagrangian multipliers of the system. Rearranging these equations results in

$$\mu = -\frac{x_3\lambda_3 + x_4\lambda_4}{{x_3}^2 + {x_4}^2}\,, \tag{5.35}$$

$$u_1 = -\lambda_3 + x_3\frac{x_3\lambda_3 + x_4\lambda_4}{{x_3}^2 + {x_4}^2}\,, \tag{5.36}$$

$$u_2 = -\lambda_4 + x_4\frac{x_3\lambda_3 + x_4\lambda_4}{{x_3}^2 + {x_4}^2}\,. \tag{5.37}$$

Modifications to the Euler-Lagrange equations, which determine the optimality conditions, are also necessary to develop the costate equations and are derived from

$$\dot{\boldsymbol{\lambda}}^T = -H_{\boldsymbol{x}} = -{\mathcal{L}_{\boldsymbol{x}}}^T - {\boldsymbol{f}_{\boldsymbol{x}}}^T\boldsymbol{\lambda} - {C_{\boldsymbol{x}}}^T\mu\,. \tag{5.38}$$

Carrying out the derivation yields

$$\dot{\boldsymbol{\lambda}}^T = -\begin{bmatrix}\mathcal{L}_{x_1}\\ \mathcal{L}_{x_2}\\ \mathcal{L}_{x_3}\\ \mathcal{L}_{x_4}\end{bmatrix} - \begin{bmatrix}\frac{\partial f_1}{\partial x_1} & \frac{\partial f_2}{\partial x_1} & \frac{\partial f_3}{\partial x_1} & \frac{\partial f_4}{\partial x_1}\\ \frac{\partial f_1}{\partial x_2} & \frac{\partial f_2}{\partial x_2} & \frac{\partial f_3}{\partial x_2} & \frac{\partial f_4}{\partial x_2}\\ \frac{\partial f_1}{\partial x_3} & \frac{\partial f_2}{\partial x_3} & \frac{\partial f_3}{\partial x_3} & \frac{\partial f_4}{\partial x_3}\\ \frac{\partial f_1}{\partial x_4} & \frac{\partial f_2}{\partial x_4} & \frac{\partial f_3}{\partial x_4} & \frac{\partial f_4}{\partial x_4}\end{bmatrix}\begin{bmatrix}\lambda_1\\ \lambda_2\\ \lambda_3\\ \lambda_4\end{bmatrix} - \begin{bmatrix}C_{x_1}\\ C_{x_2}\\ C_{x_3}\\ C_{x_4}\end{bmatrix}\mu\,, \tag{5.39}$$

$$\dot{\boldsymbol{\lambda}}^T = -\begin{bmatrix}0\\0\\0\\0\end{bmatrix} - \frac{\partial}{\partial \boldsymbol{x}}\left(\begin{bmatrix}0&0&1&0\\0&0&0&1\\0&0&0&0\\0&0&0&0\end{bmatrix}\begin{bmatrix}x_1\\x_2\\x_3\\x_4\end{bmatrix} + \begin{bmatrix}0&0\\0&0\\1&0\\0&1\end{bmatrix}\begin{bmatrix}u_1\\u_2\end{bmatrix}\right)^T\begin{bmatrix}\lambda_1\\\lambda_2\\\lambda_3\\\lambda_4\end{bmatrix} - \mu\frac{\partial}{\partial \boldsymbol{x}}\left[x_3u_1 + x_4u_2\right], \tag{5.40}$$

$$\begin{bmatrix}\dot{\lambda}_1\\\dot{\lambda}_2\\\dot{\lambda}_3\\\dot{\lambda}_4\end{bmatrix} = -\tfrac{\partial}{\partial \boldsymbol{x}}\begin{bmatrix}x_3 & x_4 & u_1 & u_2\end{bmatrix}\begin{bmatrix}\lambda_1\\\lambda_2\\\lambda_3\\\lambda_4\end{bmatrix} - \mu\tfrac{\partial}{\partial \boldsymbol{x}}\left[x_3u_1 + x_4u_2\right]\,, \tag{5.41}$$

$$\begin{bmatrix}\dot{\lambda}_1\\\dot{\lambda}_2\\\dot{\lambda}_3\\\dot{\lambda}_4\end{bmatrix} = -\tfrac{\partial}{\partial \boldsymbol{x}}\left[x_3\lambda_1 + x_4\lambda_2 + u_1\lambda_3 + u_2\lambda_4\right] - \mu\tfrac{\partial}{\partial \boldsymbol{x}}\left[x_3u_1 + x_4u_2\right]\,, \tag{5.42}$$

simplifying finally to

$$\begin{bmatrix} \dot{\lambda}_1 \\ \dot{\lambda}_2 \\ \dot{\lambda}_3 \\ \dot{\lambda}_4 \end{bmatrix} = - \begin{bmatrix} 0 \\ 0 \\ \lambda_1 \\ \lambda_2 \end{bmatrix} - \mu \begin{bmatrix} 0 \\ 0 \\ u_1 \\ u_2 \end{bmatrix} . \tag{5.43}$$

Substituting $\dot{x}_4$ and $\dot{x}_5$ for u_1 and u_2 results in the fully defined equations governing the optimal trajectory and the input which generates this path while satisfying the constraints.

$$\mu = -\frac{x_3\lambda_3 + x_4\lambda_4}{{x_3}^2 + {x_4}^2} \tag{5.44}$$

$$u_1 = -\lambda_3 - x_3\mu \tag{5.45}$$

$$u_2 = -\lambda_4 - x_4\mu \tag{5.46}$$

$$\dot{x}_1 = \quad x_3 \tag{5.47}$$

$$\dot{x}_2 = \quad x_4 \tag{5.48}$$

$$\dot{x}_3 = \quad u_1 \tag{5.49}$$

$$\dot{x}_4 = \quad u_2 \tag{5.50}$$

$$\dot{\lambda}_1 = \quad 0 \tag{5.51}$$

$$\dot{\lambda}_2 = \quad 0 \tag{5.52}$$

$$\dot{\lambda}_3 = -\lambda_1 - \dot{x}_3\mu \tag{5.53}$$

$$\dot{\lambda}_4 = -\lambda_2 - \dot{x}_4\mu \tag{5.54}$$

When μ equals zero, these governing equations collapse to the equations of motion without an equality constraint on the velocity state.

These dynamic equations are integrated in time from an initial time and boundary conditions to a final state using MATLAB.[72] However, the solution does not ensure that the final boundary conditions are satisfied. For this reason, the following nonlinear least squares problem is posed to find the values of the initial Lagrangian multipliers required to achieve the desired final boundary conditions. Using the final aircraft state values at the end of the simulation, the following objective function can be formed

$$F\left(\boldsymbol{\lambda}_0\right) = \sum_{i=1}^{N} \left\| x_i(t_f) - x_{i,f} \right\|^2 \tag{5.55}$$

in which $\boldsymbol{\lambda}_0 = \boldsymbol{\lambda}(t_0)$ is the initial Lagrangian multiplier vector, $x_i(t_f)$ is the simulated final ith state of the aircraft, $x_{i,f}$ is the desired final ith state, N is the number of states, and the function, $F(\boldsymbol{\lambda}_0)$, is computed from the simulation. The Levenburg-Marquardt method, implemented in MATLAB by `lsqnonlin`,[73] is used to solve this system of equations for

the appropriate initial Lagrangian multipliers. Note that this problem is not a traditional least squares problem because the final state boundary condition error in Eq. (5.55) can be reduced precisely to zero.

5.3 ACOUSTIC CONSTRAINT INCORPORATION

A comprehensive description of how the Observer Sound Pressure Model was developed was provided in Chapter 3. A description of how that model will be integrated into the trajectory optimization will now be provided in this section. Then, the nominal trajectory to be used in all simulations will be described, followed by a discussion of the Observer Sound Pressure Model with uniform directivity considered.

5.3.1 Method

The first step in modifying the trajectory of the aircraft to account for observer noise is to calculate an optimal minimum time nominal trajectory such as the one shown in Fig. 3.5, neglecting the acoustic constraint. In this figure, the flight segment begins spatially at (0,0) m and ends at (1000, 200) m, and the aircraft model flies directly over the acoustic observer at (500, 100) m. The flight path is not a straight line due to the boundary constraints on x and y velocity components. This path results in the maximum SPL that the observer could experience as this would result in the shortest aircraft-to-observer distance as the aircraft flies at a constant altitude directly over the observer. This process is fully contained within the optimization trajectory function and minimize time decision blocks shown in Fig. 5.2. A MATLAB[72] script creates a time series vector containing the SPL at the acoustic observer during the flight segment, from which the maximum SPL is saved. This maximum SPL is used as a baseline value from which a more acceptable noise level at the observer can be targeted.

Once the baseline value is determined, a desired SPL reduction at the observer can be specified. If the SPL reduction is not satisfied, then the flight duration is increased and the optimization is repeated. Increasing the flight duration forces the flight trajectory to bulge away from the acoustic observer, with a corresponding reduction in SPL at the observer. Note that the trajectory optimization is performed independent of the acoustics, and that incorporating the acoustic constraint is an additional step, as shown in Fig. 5.2. If the SPL reduction is satisfied, then the flight duration is reduced to see if a shorter flight trajectory can be found that satisfies the SPL target. If the specified time is so short that no solution can be found, then the time is increased. Adaptive gain logic is also included that will reduce the change in flight duration if it is necessary to have a smaller change in SPL. This method

is an iterative process that continues until the desired SPL reduction is met with a tolerance of 0.25 dB or 25 iterations are reached. While the use of a tolerance less than 0.25 dB is mathematically possible, it is not reasonable as a human observer can barely distinguish a 3 dB difference in sound levels.

5.4 SIMULATION RESULTS

This section will present the results of simulations performed using the algorithm developed to optimize a trajectory using the uniform directivity Observer Sound Pressure Model. First, the nominal trajectory is described. Then, results of simulations to reduce observer SPL from the baseline value will be presented, analyzed, and compared.

5.4.1 Nominal Trajectory

To analyze the effectiveness of incorporating the Observer Sound Pressure Model into the trajectory optimization algorithm, it is necessary to first define a baseline flight segment from which all simulations will be performed. The initial and final flight conditions for the flight segment are

$$\boldsymbol{x}_0 = [\,0\;\; 0\;\; \nu\cos\chi_0\;\; \nu\sin\chi_0\,]^T\,(\text{m, m/s})\;, \tag{5.56}$$

$$\boldsymbol{x}_f = [\,1000\;\; 200\;\; \nu\cos\chi_f\;\; \nu\sin\chi_f\,]^T\,(\text{m, m/s})\;, \tag{5.57}$$

in which $\boldsymbol{x}_0 = \boldsymbol{x}(t_0)$ is the initial state, $\boldsymbol{x}_f = \boldsymbol{x}(t_f)$ is the final state, ν is the nominal flight speed of 30 m/s, χ_0 is the initial heading angle of 0°, χ_f is the final heading angle of 0°. An acoustic observer is placed at (500, 100) m on the ground. To analyze the acoustic effects on the ground plane, 1500 points in the vicinity of the trajectory are used to form a grid that encompasses the ground plane of the trajectory. The Observer Sound Pressure Model is used to calculate the SPL at every time step and grid point on the ground plane based on the aircraft flying at a constant altitude of 30 m. The flight duration was based on the determined minimum control effort generated trajectory, resulting in a time of 34 s. This method is highly dependent on boundary conditions and the flight duration may change dramatically for other initial and final states.

5.4.2 Simulations

Results of the nominal trajectory and five noise reduction simulations are presented in Tab. 5.1; respective trajectories are plotted in Fig. 5.3. These results include the desired

Table 5.1 Summary of Attempts to Reduce Observer Noise

$\Delta L_{\text{max, desired}}$ (dB ref. p_0)	L_{max} (dB ref. p_0)	$\Delta L_{\text{max, actual}}$ (dB ref. p_0)	t_f (sec)	Δt_f (sec)
0	51.42	0	34.05	0
-5	46.47	-4.95	34.49	0.44
-10	41.41	-10.01	35.02	0.97
-15	36.47	-14.95	36.68	2.63
-20	31.63	-19.79	47.49	13.44
-25	31.44	-19.98	67.49	33.44

maximum observer SPL reduction ($\Delta L_{\text{max, desired}}$), calculated maximum SPL (L_{max}), maximum SPL reduction achieved (ΔL_{max}), flight duration (t_f), and change in flight duration from the nominal (Δt_f).

The nominal trajectory corresponds to the first row of Tab. 5.1 and the blue trajectory in Fig. 5.3, in which the vehicle flew directly over the acoustic observer. This trajectory resulted in a maximum SPL at the observer of 51 dB and a flight duration of 34 s. As the desired maximum SPL was reduced in subsequent simulations, the iterative algorithm increased the flight time, thereby forcing the trajectory to curve away from the observer and decreasing the maximum observer SPL. This trend is apparent in Tab. 5.1; as the flight times in columns 4 and 5 increase, the maximum observer SPL decreases proportionally for most of the simulations presented.

Results for a 15 dB reduction in maximum observer SPL are shown in the 4th row of Tab. 5.1 and correspond to the purple trajectory in Fig. 5.3. To satisfy the noise reduction goal, the iterative algorithm increased the flight time by 2.63 s, creating a trajectory that curved away from the observer. This curved trajectory resulted in the maximum SPL contour shown in Fig. 5.4.

The results for a 20 dB reduction in maximum observer SPL are presented in the 5th row of Tab. 5.1 and the green trajectory in Fig. 5.3. The actual reduction in observer SPL was the desired 20 dB with an increased flight duration of 13 s. Observe in Fig. 5.3 that the trajectory curved much further away from the acoustic observer when compared to the 5, 10, and 15 dB reduction trajectories. The ground contour plot (see Fig. 5.5) suggests that the maximum observer SPL was a result of the vehicle flying closer to the acoustic observer to satisfy the final boundary conditions (BCs). Evidence to support this suggestion is presented below.

The trajectory generation process worked well for the previous cases, but failed to satisfy the BCs and the acoustic constraint when attempting to reduce the maximum observer SPL by 25 dB, which corresponds to the 6th row of Tab. 5.1 and the light blue trajectory in Fig. 5.3. The actual maximum SPL reduction in this simulation was 20 dB and the flight

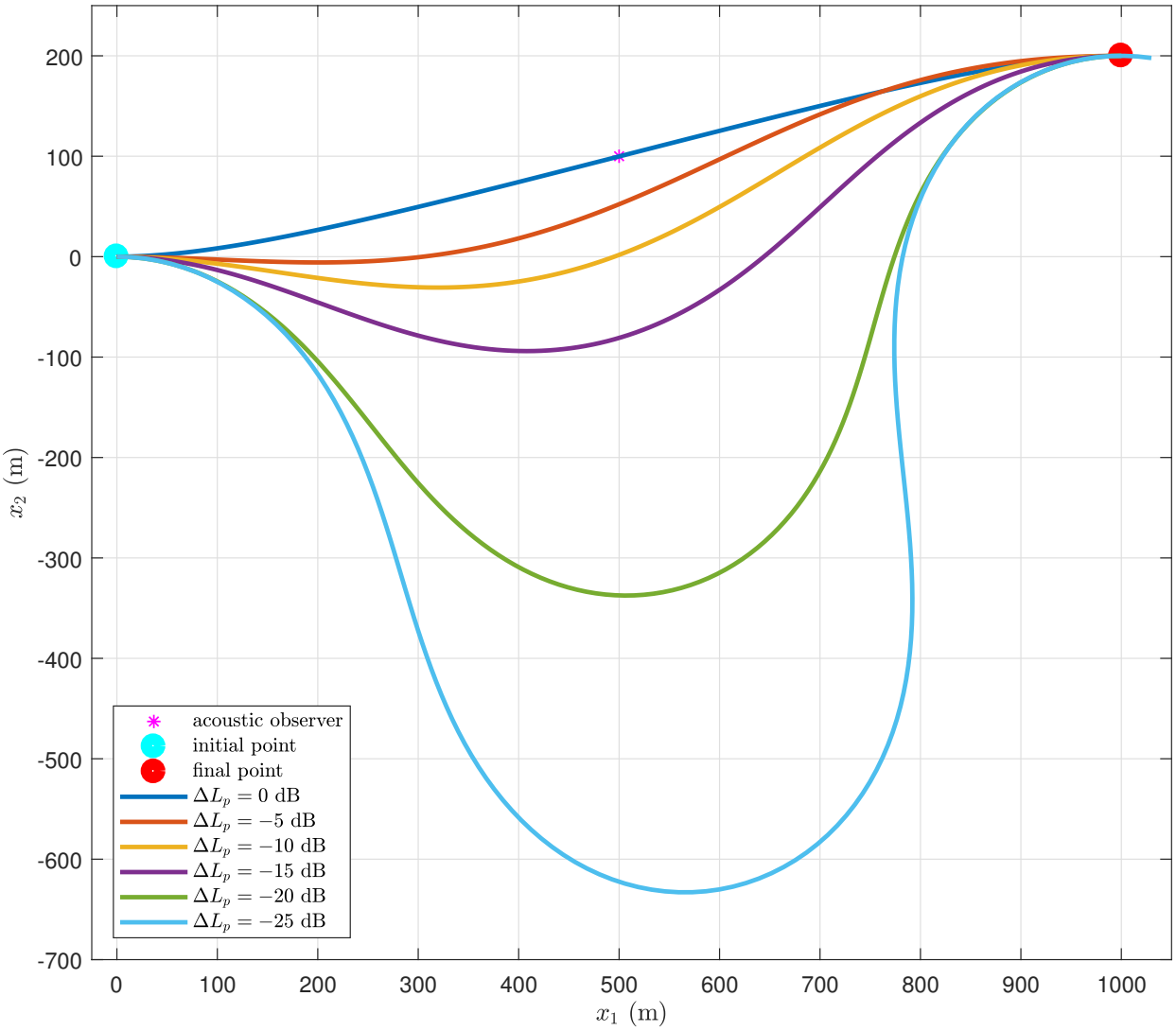

Figure 5.3 Trajectories with Various Maximum Sound Pressure Levels at an Observer

duration increased by 33 s. Observe in Fig. 5.6 that the maximum SPL at the acoustic observer was due to the vehicle operating near the point $(800, 50)$ m to satisfy the final BCs. The optimization algorithm attempted to calculate a trajectory that would satisfy the acoustic constraint, but the process could not find a solution within the 25-iteration limit described in §5.3. As a result, the process failed to generate a trajectory that satisfied both the time constraint and the final BCs. The trajectory solution at the 25th iteration, shown in Fig. 5.3 in light blue, extended past the final point on the flight path. Increasing the 25-iteration limit only increased the flight duration without a reduction in maximum observer SPL. Evidence to support this is presented in Fig. 5.7, in which the optimization framework calculates new trajectories with longer flight times in an attempt to satisfy the target maximum observer SPL. Note that the trajectories converge near the point $(800, 50)$ m, and due

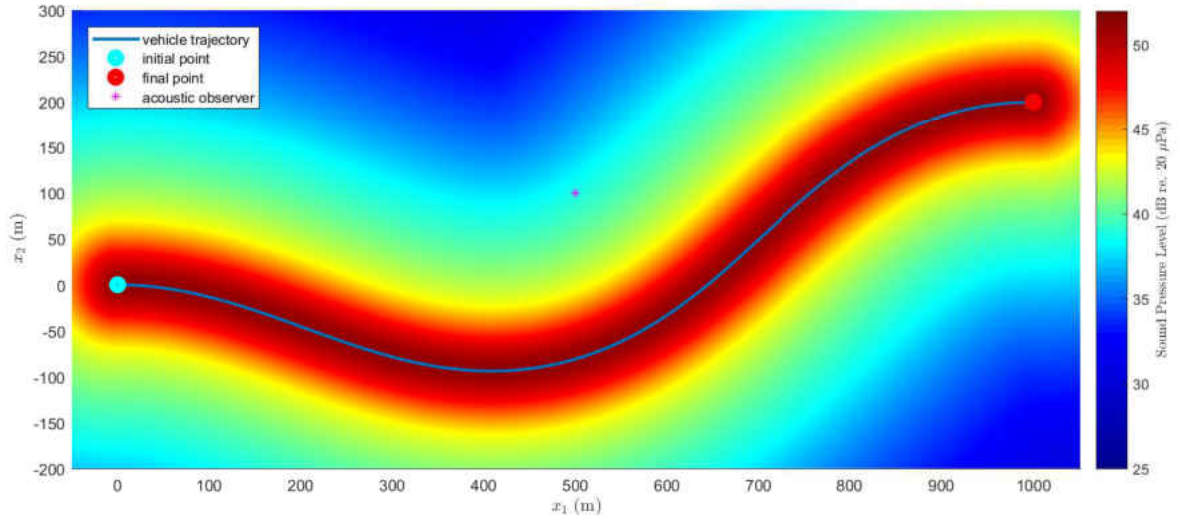

Figure 5.4 Optimal Trajectory and Maximum SPL Contour for Desired Reduction of 15 dB at the Observer

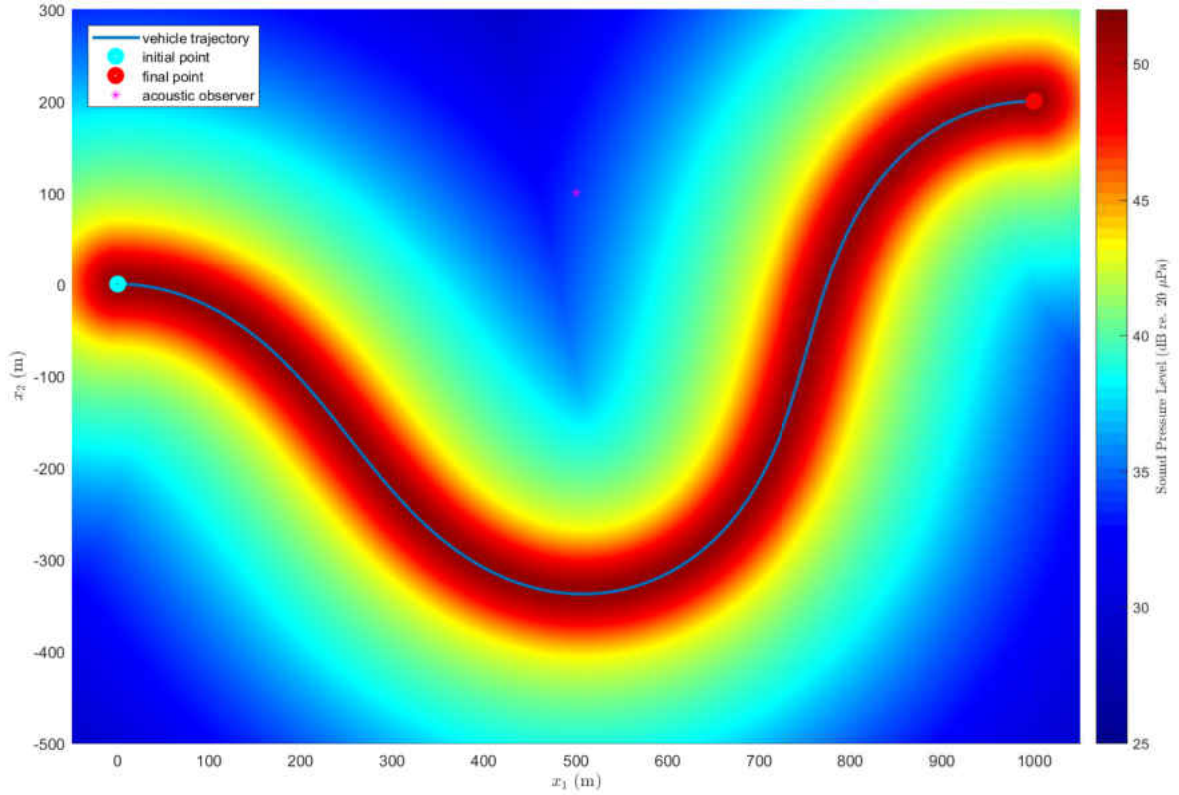

Figure 5.5 20 dB Maximum SPL Reduction at the Acoustic Observer Compared to the Nominal Trajectory

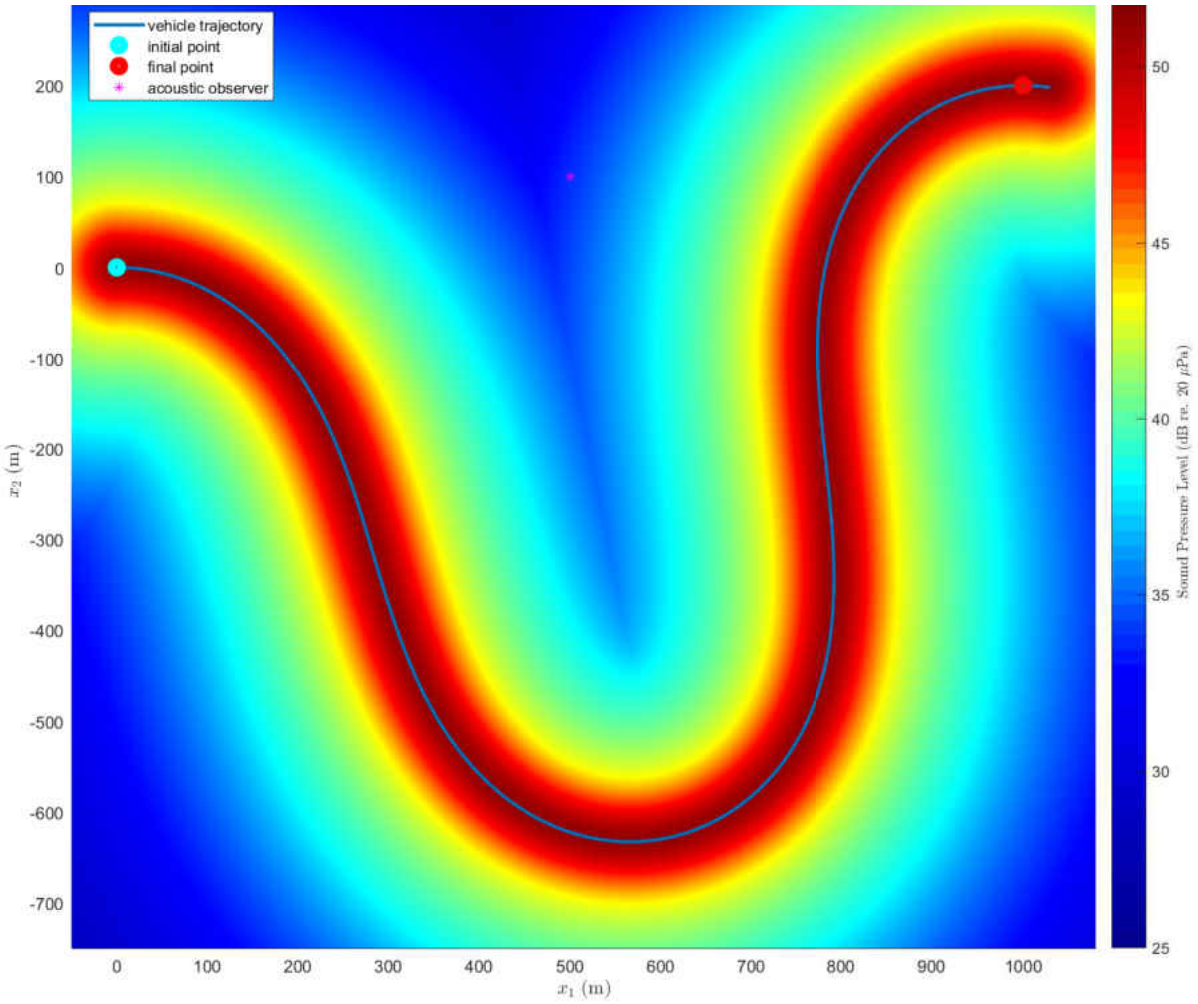

Figure 5.6 Failed Attempt to Reduce Maximum Sound Pressure Level by 25 dB, Final Result

to the proximity to the observer, the desired maximum observer SPL cannot be satisfied. In this scenario, curving the trajectory away from the acoustic observer provided no further acoustic benefit and only resulted in increased flight time.

5.5 LIMITATIONS

Several limitations with the work presented in this chapter are considered. Indirect optimization requires an initial investment to manually derive the differential equations that govern the change in both Lagrangian multipliers and state variables throughout the simulation. Sometimes it can be extremely difficult or not feasible to find a closed-form solution. For this reason, it is very difficult to incorporate an acoustic model directly into the cost function for the optimization framework. In this case, a separate derivation of the equations of motion are required for each acoustic model used due to the differentiation of the cost

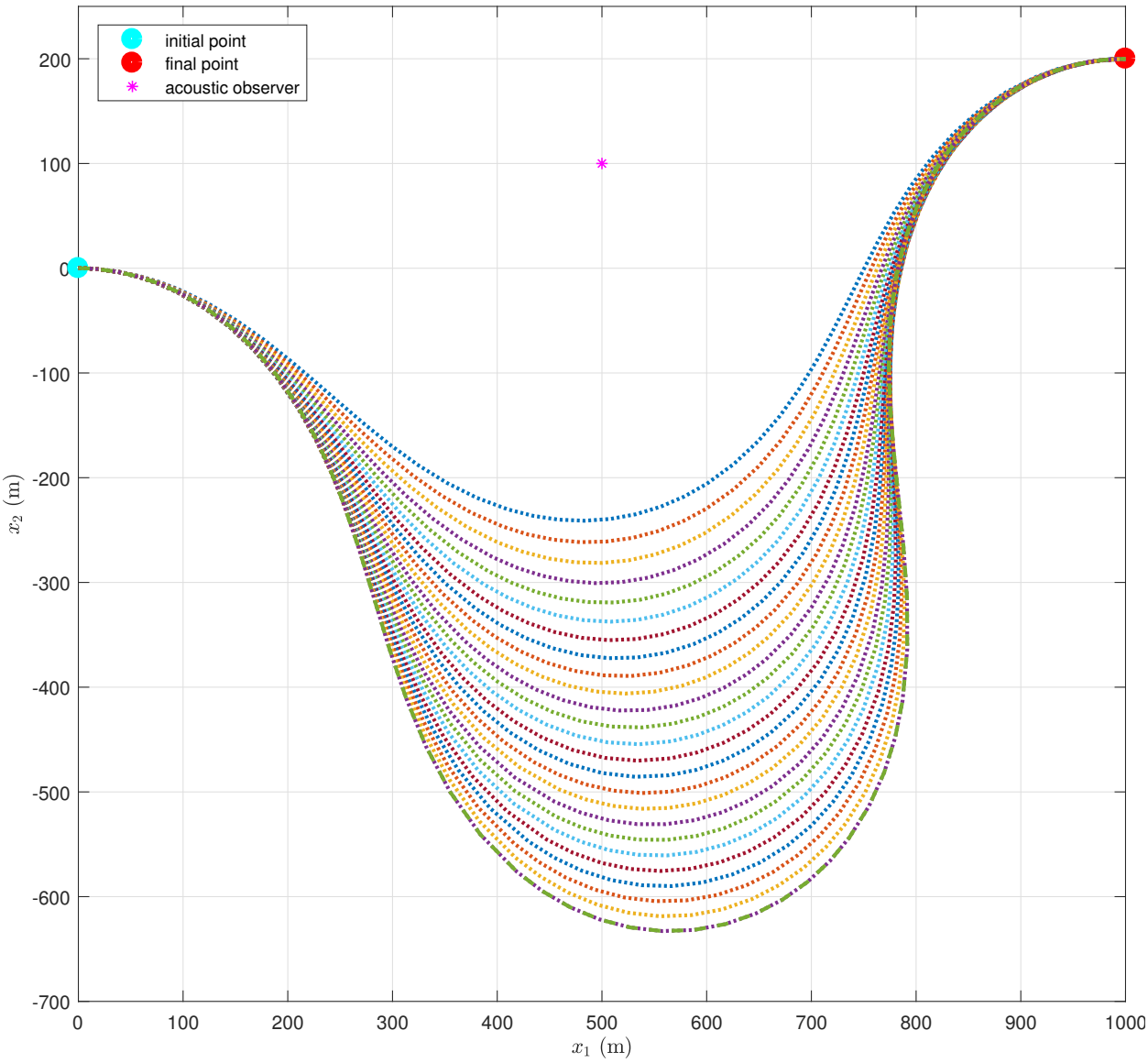

Figure 5.7 Failed Attempts to Reduce Maximum Sound Pressure Level by 25 dB, Iteration History

function and acoustic model with respect to time and the states. This issue is compounded as more complicated (and potentially more realistic) acoustic models are used.

Another limitation to the framework developed is that it is not a robust optimization system and is quite susceptible to not only the initial conditions of the states, but also the determined final time and the flight velocity. A solver is used to determine the initial Lagrangian multipliers to satisfy the boundary conditions, and the optimal equations are simply propagated through time to do this. For the current framework, it is impossible to dynamically change the equations midsimulation. Dynamic programming is used to determine a minimum-time solution only after the optimal trajectory is calculated. The ability

to dynamically change the governing equations would be useful to avoid cases in which the optimization algorithm converges on a solution that violates the desired SPL constraint. For instance, when specifying a constant flight velocity of 25 m/s, the minimization of time routine converged on a solution that created a trajectory in which the aircraft flew directly over the observer, violating the specified sound constraint. An increase in robustness would be required in order to develop this framework further.

The equations of motion chosen for this work comprise a simple double integrator system for a simple point mass aircraft model. For this feasibility study, this assumption may be appropriate but a more realistic aircraft model may be necessary in future work. This issue is also found in the Observer Sound Pressure Model, which could be substituted with a more accurate semiempirical model instead of the current one that represents isolated propellers. Lastly, a barrier to production use of this framework is the computational effort. The computation time for these simulations prevent the creation of an optimal trajectory in real time, and the computation time would only increase as more accurate or realistic aircraft and acoustic models are implemented.

5.6 SUMMARY

In this chapter, background theory in optimal control was presented and applied to a two-dimensional double integrator system. Then, dynamic programming was developed to set an acoustic constraint on the maximum SPL that an observer experiences during a fly-by flight segment. Six separate cases were evaluated for a specific scenario, which included a nominal minimum-time trajectory, as well as five attempts to reduce the maximum SPL by 5 dB, 10 dB, 15 dB, 20 dB, and finally 25 dB. The first four attempts to constrain the observer were successful. However, the last simulation was not successful due to the fact that the aircraft violated the acoustic constraint during its approach to the final boundary condition. The SPL exceeded the specified constraint, and the algorithm continued to increase the flight time until a specified maximum number of iterations was reached.

While there are limitations to consider, this investigation demonstrated the capability that acoustics can be considered during the path planning process, specifically when developing an optimized trajectory that minimizes control effort and time to destination.

CHAPTER 6
SUMMARY

This thesis presented two methods to reduce or mitigate the effects of noise from a UAS. The first method integrated a model of the source noise into a flight control system to modify the flight parameters of a vehicle, directly modifying the noise emission of the aircraft. The second method considered an observer noise model, estimating the noise experienced by an observer to modify the planned trajectory of an aircraft. The rest of this chapter will review the chapters in this thesis, provide a summary of results, and contributions to the academic community.

6.1 CHAPTER REVIEW

In Chapter 2, a review of the vehicle system used in this work was presented and an overview of each subsystem was discussed. This review included a flight dynamics controller, a path-following controller, and the vehicle dynamics model. Additionally, an energy consumption model was developed for use in subsequent chapters. This energy consumption model quantifies how modifying the flight parameters affects the efficiency and energy consumption of the vehicle.

Chapter 3 discussed the acoustic models developed for the current work. First, the Source Sound Power Model was developed that estimates the sound power level of the GL-10 as it operates during a mission. This model was compared to a surrogate model developed using ANOPP-PAS. Then, the Observer Sound Pressure Model was developed to estimate the sound pressure level that an observer experiences during a flyover event. This model was further simplified to assume uniform directivity and provides a more conservative estimate of sound pressure level. These models were developed based on theory developed in the early part of the 20th century, but are appropriate for demonstrating the capability of reducing the noise of a vehicle through the control system. As a result, a high accuracy acoustic model is not of primary importance.

In Chapter 4, the Source Sound Power Model was integrated into the vehicle system described in Chapter 2 to create a rudimentary acoustically-aware vehicle. This integration led to the creation of an acoustic controller that modified the flight velocity command of the vehicle, which in turn modified the source noise of the vehicle to meet some specified criteria. Simulations performed showed that this strategy was one method to reduce the generated noise of the aircraft.

In the last chapter, Chapter 5, a trajectory was optimized using optimal control meth-

ods and dynamic programming to satisfy three metrics: (i) minimize control effort, (ii) minimize time in flight, and (iii) achieve a desired SPL reduction. First, an optimal solution was determined to minimize the aircraft model's control effort during a flight segment. Then, the algorithm minimized the time in flight for given initial and final conditions on position and velocity. Finally, dynamic programming was used to increase or decrease the flight time based on the SPL that an observer experienced, which resulted in a modified trajectory. Simulations demonstrated the capability of reducing aircraft noise imposed on an observer during the path planning process.

6.2 RESULTS SUMMARY

A research question was posed at the beginning of this thesis – "How do we reduce aircraft noise at an observer by means of flight control system augmentation?" To answer this research question, two methods were proposed to reduce observer noise. The first method demonstrated that it is possible to interact directly with a preexisting flight control system and modify the speed of the aircraft to reduce noise. A limitation of this method is that flight speed must be an input to the path-following controller or the flight control system. The second method demonstrated that it is possible to optimize a trajectory during the path planning process to spatially avoid an acoustic observer (or even an acoustically sensitive region). A few limitations of this method include: (i) it is computationally expensive, thus, not suitable for real time path planning, (ii) it is very sensitive to boundary conditions, and (iii) the acoustic model is incorporated via dynamic programming instead of directly embedded in the cost function. Both of the methods presented offer feasible solutions to the research problem previously posed.

6.3 CONTRIBUTIONS

The research that has accumulated into the bulk of this thesis has been or will be disseminated to the research community through public conferences. Namely, the work that makes up the bulk of Chapter 4 was presented at the AIAA Hampton Roads Section (HRS) Second Annual Spring Student Research Forum at the NASA Langley Research Center and the 24th AIAA/CEAS Aeroacoustics Conference held at the 2018 AIAA Aviation Forum in Atlanta, Georgia.[74] The research contained within Chapter 5 will be submitted for consideration to the 26th AIAA/CEAS Aeroacoustics Conference to be held at the 2020 AIAA Aviation Forum in Reno, Nevada.[75] The full citations for the aforementioned presentations or publications are:

1. Galles, M. B., "Closed-Loop Feedback Control of Flight Speed to Reduce Unmanned Aerial System Noise: Current Progress," *AIAA HRS Second Annual Spring Student Research Forum*, Hampton, Virginia, March, 2018,

2. Galles, M. B., Schiller, N. H., Ackerman, K. A., and Newman, B., "Feedback Control of Flight Speed to Reduce Unmanned Aerial System Noise," *Proceedings of the 24th AIAA/CEAS Aeroacoustics Conference*, AIAA Aviation Forum, Atlanta, Georgia, June, 2018
doi: 10.2514/6.2018-2950 AIAA 2018-2950

3. Galles, M. B. and Newman, B., "Reducing the Noise Impact of Small Aircraft through Indirect Trajectory Optimization," *Proceedings of the 26th AIAA/CEAS Aeroacoustics Conference*, AIAA Aviation Forum, Reno, Nevada, June, 2020 (to be submitted).

6.4 FUTURE WORK

For the first part of the work contained herein, future work would include changing the acoustic targets to spatial constraints instead of temporal targets and incorporating a time lead feature to anticipate upcoming acoustic zones. Additionally, only the flight speed was considered for modification but modifying the roll, pitch, and yaw of the aircraft could be another method to direct noise away from an observer during a mission.

For the path planning component of this thesis, the current work optimizes a trajectory based on equations of motion and a cost function that minimizes control effort. Future work would incorporate the acoustic metric and model directly into the cost function itself. Additionally, it would be beneficial to create a separate cost function that only operates when the constraint is violated. Modern optimization techniques or software could be used instead of traditional optimal control theory, such as OpenMDAO.[76] Lastly, robustness of the framework would need to be increased to reduce the sensitivity of the current optimization scheme to initial conditions and flight parameters.

The methods contained in this work could be combined such that the flight parameters are modified in tandem with optimization of the trajectory, or a combination of the work contained herein with work performed by Pascioni et al.[77] This concept could include modification of the phase between propellers to affect the directivity of generated noise.

REFERENCES

[1] Münzel, T., Schmidt, F. P., Steven, S., Herzog, J., Daiber, A., and Sørensen, M., "Environmental Noise and the Cardiovascular System," *Journal of the American College of Cardiology*, Vol. 71, No. 6, Februrary, 2018, pp. 688–697.
doi: 10.1016/j.jacc.2017.12.015.

[2] Basner, M., Clark, C., Hansell, A., Hileman, J. I., Janssen, S., Shepherd, K., and Sparrow, V., "Aviation Noise Impacts: State of the Science," *Noise & Health*, Vol. 19, No. 87, 2017, pp. 41–50.

[3] Kaltenbach, M., Maschke, C., and Klinke, R., "Health Consequences of Aircraft Noise," *Deutsches Arzteblatt International*, Vol. 105, No. 31–32, 2008, pp. 548–556.
doi: 10.3238/arztebl.2008.0548.

[4] Correia, A. W., Peters, J. L., Levy, J. I., Melly, S., and Dominici, F., "Residential Exposure to Aircraft Noise and Hospital Admissions for Cardiovascular Diseases: Multi-airport Retrospective Study," *BMJ (Clinical research ed.)*, Vol. 347, No. 7928, October, 2013.
doi: 10.1136/bmj.f5561.

[5] Thomas, J., Jensen, L., Brooks, C., Brenner, M., Salgueiro, S., and Hansman, R. J., "Investigation of Aircraft Approach and Departure Velocity Profiles on Community Noise," *Proceedings of the 23rd AIAA/CEAS Aeroacoustics Conference*, AIAA Aviation Forum, Denver, Colorado, June, 2017.
doi: 10.2514/6.2017-3188, AIAA 2017-3188.

[6] Sahai, A. K., Snellen, M., Simons, D. G., and Stumpf, E., "Aircraft Design Optimization for Lowering Community Noise Exposure Based on Annoyance Metrics," *Journal of Aircraft*, Vol. 54, No. 6, 2017, pp. 2257–2269.
doi: 10.2514/1.C034009.

[7] Leifsson, L., Mason, W., Schetz, J., Haftka, R., and Grossman, B., "Multidisciplinary Design Optimization of Low-Airframe-Noise Transport Aircraft," *Proceedings of the 44th AIAA Aerospace Sciences Meeting and Exhibit*, AIAA, Reno, Nevada, January, 2006.
doi: 10.2514/6.2006-230, AIAA 2006-230.

[8] Martens, S., "Jet Noise Reduction Technology Development at GE Aircraft Engines," *Proceedings of the 23rd International Congress of Aeronautical Sciences*, ICAS, Toronto, Ontario, Canada, September, 2002. ICAS 2002-8.4.2.

[9] Brausch, J. F., Janardan, B. A., Barter IV, J. W., and Hoff, G. E., "Chevron Exhaust Nozzle for a Gas Turbine Engine," US Patent No. 6,360,528 B1, 2002.

[10] Blodgett, K. E. J., Early, K. S., Martens, S., Bailey, W. A., and Price, K. D., "Sinuous Chevron Exhaust Nozzle," US Patent No. 7,305,817 B2, 2007.

[11] Feuillard, P., Hemeury, P., and Gerri, C., "Chevron-Type Primary Exhaust Nozzle for Aircraft Turbofan Engine, and Aircraft Comprising such a Nozzle," US Patent No. 7.469,529 B2, 2008.

[12] Ozcan, H. and Nemlioglu, S., "In-Cabin Noise Levels During Commercial Aircraft Flights," *Canadian Acoustics*, Vol. 34, No. 4, December, 2006, pp. 31–35.

[13] Elliot, S. J., Nelson, P. A., Stothers, I. M., and Boucher, C. C., "In-Flight Experiments on the Active Control of Propeller-Induced Cabin Noise," *Journal of Sound and Vibration*, Vol. 140, No. 2, 1990, pp. 219–238.
doi: 10.1016/0022-460X(90)90525-5.

[14] Fuller, C. R. and von Flotow, A. H., "Active Control of Sound and Vibration," *IEEE Control Systems*, Vol. 15, No. 6, 1995, pp. 9–19.
doi: 10.1109/37.476383.

[15] Schiller, N. H., Cabell, R. H., Quinones, J. D., and Wier, N. C., "Active Damping Using Distributed Anisotropic Actuators," *Proceedings of the ASME 2010 International Mechanical Engineering Congress & Exposition*, Vancouver, British Colombia, Canada, November, 2010, pp. 73–80.
doi: 10.1115/IMECE2010-37503.

[16] Seebass, R., "Sonic Boom Theory," *Journal of Aircraft*, Vol. 6, No. 3, 1969, pp. 177–184.
doi: 10.2514/3.44032.

[17] Ordaz, I. and Li, W., "Integration of Off-Track Sonic Boom Analysis for Supersonic Aircraft Conceptual Design," *Journal of Aircraft*, Vol. 51, No. 1, 2014, pp. 23–28.
doi: 10.2514/1.C031511.

[18] Lim, T., Sankar, L., Hariharan, N., and Reddy, N., "A Technique for the Prediction of Propeller Induced Acoustic Loads on Aircraft Surfaces," *Proceedings of the 15th AIAA Aeroacoustics Conference*, AIAA, Long Beach, California, October, 1993.
doi: 10.2514/6.1993-4340, AIAA 1993-4340.

[19] Vaicaitis, R. and Dowell, E. H., "Response of Space Shuttle Surface Insulation Panels to Acoustic Pressure," *Journal of Spacecraft and Rockets*, Vol. 14, No. 12, 1977, pp. 739–746.

[20] Plotkin, K. J., "Sonic Boom Focal Zones from Tactical Aircraft Maneuvers," *Journal of Aircraft*, Vol. 30, No. 1, 1993, pp. 75–80.
doi: 10.2514/3.46308.

[21] Hoehne, V. O. and Luce, R. G., "The Quieted Aircraft as a Military Tool," *Proceedings of the AIAA Aircraft Design and Operations Meeting*, AIAA, Los Angeles, California, July, 1969.
doi: 10.2514/6.1969-792, AIAA 1969-792.

[22] Epstein, A. H., "Distributed Propulsion: New Opportunities for an Old Concept," Final Report, DARPA Contract HR001-07-C-0005, Gas Turbine Laboratory, Massachusetts Institute of Technology, Cambridge, Massachusetts, December, 2007.

[23] Gohardani, A. S., "A Synergistic Glance at the Prospects of Distributed Propulsion Technology and the Electric Aircraft Concept for Future Unmanned Air Vehicles and Commercial/Military Aviation," *Progress in Aerospace Sciences*, Vol. 57, February, 2013, pp. 25–70.
doi: 10.1016/j.paerosci.2012.08.001.

[24] Kirner, R., Raffaelli, L., Rolt, A., Laskaridis, P., Doulgeris, G., and Singh, R., "An Assessment of Distributed Propulsion: Advanced Propulsion System Architectures for Conventional Aircraft Configurations," *Aerospace Science and Technology*, Vol. 46, October–November, 2015, pp. 42–50.
doi: 10.1016/j.ast.2015.06.022.

[25] Wick, A. T., Hooker, J. R., and Zeune, C. H., "Integrated Aerodynamic Benefits of Distributed Propulsion," *Proceedings of the 53rd AIAA Aerospace Sciences Meeting*, AIAA SciTech Forum, Kissimmee, Florida, January, 2015.
doi: 10.2514/6.2015-1500, AIAA 2015-1500.

[26] Christian, A. W. and Cabell, R., "Initial Investigation into the Psychoacoustic Properties of Small Unmanned Aerial System Noise," *Proceedings of the 23rd AIAA/CEAS Aeroacoustics Conference*, AIAA Aviation Forum, Denver, Colorado, June, 2017.
doi: 10.2514/6.2017-4051, AIAA 2017-4051.

[27] Hargest, T. J., "Noise of VTOL aircraft," *Journal of Sound and Vibration*, Vol. 4, No. 3, 1966, pp. 378–387.
doi: 10.1016/0022-460X(66)90134-9.

[28] Stepniewski, W. Z. and Schmitz, F. H., "Noise Implications for VTOL Development," *SAE Transactions*, Vol. 79, No. 2, 1970, pp. 941–956.

[29] Patterson, M. D., Antcliff, K. R., and Kohlman, L. W., "A Proposed Approach to Studying Urban Air Mobility Missions Including an Initial Exploration of Mission Requirements," *Proceedings of the AHS International 74th Annual Forum and Technology Display*, AHS, Phoenix, Arizona, May, 2018.

[30] Antcliff, K., Whiteside, S., Kohlman, L. W., and Silva, C., "Baseline Assumptions and Future Research Area for Urban Air Mobility Vehicles," *Unique and Transformational Flight, AIAA Scitech 2019 Forum*, AIAA, San Diego, California, January, 2019.
doi: 10.2514/6.2019-0528, AIAA 2019-0528.

[31] Edwards, T. E., Verma, S., and Keeler, J., "Exploring Human Factors Issues for Urban Air Mobility Operations," *Air Traffic Operations, Management, and Systems, AIAA Aviation 2019 Forum*, AIAA, Dallas, Texas, June, 2019.
doi: 10.2514/6.2019-3629, AIAA 2019-3629.

[32] Falck, R. D., Ingraham, D., Aretskin-Hariton, E., and Berton, J., "Multidisciplinary Optimization of Urban-Air-Mobility Class Aircraft Trajectories with Acoustic Constraints," *Proceedings of the 2018 AIAA/IEEE Electric Aircraft Technologies Symposium*, AIAA Propulsion and Energy Forum, Cincinnati, Ohio, July, 2018.
doi: 10.2514/6.2018-4985, AIAA 2018-4985.

[33] Johnson, W., Silva, C., and Solis, E., "Concept Vehicles for VTOL Air Taxi Operations," *Proceedings of the AHS International Technical Meeting on Aeromechanics Design for Transformative Vertical Flight*, San Francisco, California, January, 2018.

[34] Silva, C., Johnson, W. R., Patterson, M. D., and Antcliff, K. R., "VTOL Urban Air Mobility Concept Vehicles for Technology Development," *Proceedings of the 2018 Aviation Technology, Integration, and Operations Conference*, AIAA Aviation Forum, Atlanta, Georgia, June, 2018.
doi: 10.2514/6.2018-3847, AIAA 2018-3847.

[35] The MathWorks, Inc., "Simulink Ver. 8.9 (R2017a)," Natick, Massachusetts, 2017.

[36] Gutin, L. Ya., "On the Sound Field of a Rotating Propeller," NACA-TM-1195, Langley Aeronautical Laboratory, Langley Field, Virginia, October, 1948.

[37] Ffowcs Williams, J. E. and Hawkings, D. L., "Theory Relating to the Noise of Rotating Machinery," *Journal of Sound and Vibration*, Vol. 10, No. 1, 1969, pp. 10–21.
doi: 10.1016/0022-460X(69)90125-4.

[38] Mani, R., "The Radiation of Sound From a Propeller at Angle of Attack," NASA-CR-4264, Lewis Research Center, Cleveland, Ohio, January, 1990.

[39] Garrick, I. E. and Watkins, C. E., "A Theoretical Study of the Effect of Forward Speed on the Free-Space Sound-Pressure Field Around Propellers," NACA-TR-1198, Langley Aeronautical Laboratory, Langley Field, Virginia, October, 1953.

[40] Bryson, A. E. and Ho, Y. C., *Applied Optimal Control: Optimization, Estimation and Control*, Rev. ed., Taylor & Francis Group, New York, New York, 1975.
doi: 10.1002/aic.690220534.

[41] Greenwood, E., "Dynamic Replanning of Low Noise Rotorcraft Operations," *Proceedings of the Vertical Flight Society 75th Annual Forum & Technology Display*, Vertical Flight Society, Philadelphia, Pennsylvania, May, 2019.

[42] Brumitt, B. L. and Stentz, A., "Dynamic Mission Planning for Multiple Mobile Robots," *Proceedings of the 1996 IEEE International Conference on Robotics and Automation*, IEEE, Minneapolis, Minnesota, April, 1996, pp. 2396–2401.
doi: 10.1109/ROBOT.1996.506522.

[43] De Filippis, L., Guglieri, G., and Quagliotti, F., "Path Planning Strategies for UAVS in 3D Environments," *Journal of Intelligent & Robotic Systems*, Vol. 65, No. 1-4, 2012, pp. 247–264.
doi: 10.1007/s10846-011-9568-2.

[44] Li, X., Sun, Z., Cao, D., Liu, D., and He, H., "Development of a New Integrated Local Trajectory Planning and Tracking Control Framework for Autonomous Ground Vehicles," *Mechanical Systems and Signal Processing*, Vol. 87, March, 2017, pp. 118–137.
doi: 10.1016/j.ymssp.2015.10.021.

[45] Greenwood, E., II, "Fundamental Rotorcraft Acoustic Modeling from Experiments (FRAME)," Ph.D. dissertation, Dept. of Aerospace Engineering, University of Maryland, College Park, Maryland, 2011.

[46] Rothhaar, P. M., Murphy, P. C., Bacon, B. J., Gregory, I. M., Grauer, J. A., Busan, R. C., and Croom, M. A., "NASA Langley Distributed Propulsion VTOL Tilt-Wing Aircraft Testing, Modeling, Simulation, Control, and Flight Test Development," *Proceedings of the 14th AIAA Aviation Technology, Integration, and Operations Conference*, AIAA Aviation Forum, Atlanta, Georgia, June, 2014.
doi: 10.2514/6.2014-2999, AIAA 2014-2999.

[47] Fredericks, W. J., McSwain, R. G., Beaton, B. F., and Klassman, D. W., "Greased Lightning (GL-10) Flight Testing Campaign," NASA-TM-2017-219643, NASA Langley Research Center, Hampton, Virginia, July, 2017.

[48] Fredericks, W. J., Moore, M. D., and Busan, R. C., "Benefits of Hybrid-Electric Propulsion to Achieve 4x Cruise Efficiency for a VTOL UAV," *Proceedings of the 2013 International Powered Lift Conference*, AIAA Aviation Forum, Los Angeles, California, August, 2013.
doi: 10.2514/6.2013-4324, AIAA 2013-4324.

[49] Murphy, P. C., Klein, V., and Frink, N. T., "Nonlinear Unsteady Aerodynamic Modeling Using Wind-Tunnel and Computational Data," *Journal of Aircraft*, Vol. 54, No. 2, 2017, pp. 659–683.
doi: 10.2514/1.C033881.

[50] Cichella, V., Xargay, E., Dobrokhodov, V., Kaminer, I., Pascoal, A. M., and Hovakimyan, N., "Geometric 3D Path-Following Control for a Fixed-Wing UAV on SO(3)," *Proceedings of the 2011 AIAA Guidance, Navigation and Control Conference*, AIAA, Portland, Oregon, August, 2011.
doi: 10.2514/6.2011, AIAA 2011-6415.

[51] Xargay, E. M., "Time-Critical Cooperative Path-Following Control of Multiple Unmanned Aerial Vehicles," Ph.D. dissertation, Dept. of Aerospace Engineering, University of Illinois at Urbana-Champaign, Illinois, 2013.

[52] Okasha, M. and Newman, B., "Switching Algorithm to Avoid Attitude Representation Singularity," *Proceedings of the AIAA Atmospheric Flight Mechanics Conference*, AIAA, Chicago, Illinois, August, 2009.
doi: 10.2514/6.2009-6149, AIAA 2009-6149.

[53] Hovakimyan, N. and Cao, C., $\mathcal{L}_1$ *Adaptive Control Theory Guaranteed Robustness with Fast Adaptation*, Advances in Design and Control, Society for Industrial and Applied Mathematics, Philadelphia, Pennsylvania, 2010.

[54] Hovakimyan, N., Cao, C., Kharisov, E., Xargay, E., and Gregory, I. M., "$\mathcal{L}_1$ Adaptive Control for Safety-Critical Systems," *IEEE Control Systems*, Vol. 31, No. 5, 2011, pp. 54–104.
doi: 10.1109/MCS.2011.941961.

[55] Xargay, E., Hovakimyan, N., Dobrokhodov, V., Kaminer, I., Cao, C., and Gregory, I. M., "$\mathcal{L}_1$ Adaptive Control in Flight," *Advances in Intelligent and Autonomous Aerospace Systems*, edited by J. Valasek, Progress in Astronautics and Aeronautics, AIAA, Reston, Virginia, 2012, pp. 129–172.
doi: 10.2514/5.9781600868962.0129.0172.

[56] Ackerman, K. A., Xargay, E., Choe, R., Hovakimyan, N., Cotting, M. C., Jeffrey, R. B., Blackstun, M. P., Fulkerson, T. P., Lau, T. R., and Stephens, S. S., "$\mathcal{L}_1$ Stability Augmentation System for Calspan's Variable-Stability Learjet," *Proceedings of the 2016 AIAA Guidance, Navigation, and Control Conference*, AIAA SciTech Forum, San Diego, California, January, 2016.
doi: 10.2514/6.2016-0631, AIAA 2016-0631.

[57] Deming, A. F., "Propeller Rotation Noise Due to Torque and Thrust," *The Journal of the Acoustical Society of America*, Vol. 12, No. 1, 1940, pp. 173–182.
doi: 10.1121/1.1916089.

[58] Theodorsen, T. and Regier, A. A., "The Problem of Noise Reduction with Reference to Light Airplanes," NACA-TN-1145, Langley Aeronautical Laboratory, Langley Field, Virginia, August, 1946.

[59] Hubbard, H. H., "Aeroacoustics of Flight Vehicles: Theory and Practice: Volume 1: Noise Sources," NASA-RP-1258-VOL-1, NASA Langley Research Center, Hampton, Virginia, August, 1991.

[60] Zorumski, W. E. and Weir, D. S., "Aircraft Noise Prediction Program Theoretical Manual: Propeller Aerodynamics and Noise," NASA-TM-83199-PT-3, NASA Langley Research Center, Hampton, Virginia, June, 1986.

[61] White, F. A., *Our Acoustic Environment*, Wiley, New York, New York, 1975.

[62] Zawodny, N. S., Boyd, D. D., Jr., and Burley, C. L., "Acoustic Characterization and Prediction of Representative, Small-Scale Rotary-Wing Unmanned Aircraft System Components," *Proceedings of the AHS 72nd International Annual Forum and Technology Display*, AHS, West Palm Beach, Florida, May, 2016.

[63] Farassat, F. and Succi, G. P., "A Review of Propeller Discrete Frequency Noise Prediction Technology with Emphasis on Two Current Methods for Time Domain Calculations," *Journal of Sound and Vibration*, Vol. 71, No. 3, 1980, pp. 399–419.

[64] Farassat, F., "Derivation of Formulations 1 and 1A of Farassat," NASA/TM-2007-214853, NASA Langley Research Center, Hampton, Virginia, March, 2007.

[65] Brentner, K. S., "Prediction of Helicopter Rotor Discrete Frequency Noise: A Computer Program Incorporating Realistic Blade Motions and Advanced Acoustic Formulation," NASA-TM-87721, NASA Langley Research Center, Hampton, Virginia, October, 1986.

[66] Nguygen, L. C. and Kelly, J. J., "A Users Guide for the NASA ANOPP Propeller Analysis System," NASA-CR-4768, Lockheed Martin Engineering and Sciences, Hampton, Virginia, February, 1997.

[67] Pascioni, K. A. and Rizzi, S. A., "Tonal Noise Prediction of a Distributed Propulsion Unmanned Aerial Vehicle," *Proceedings of the 24th AIAA/CEAS Aeroacoustics Conference*, AIAA Aviation Forum, Atlanta, Georgia, June, 2018.
doi: 10.2514/6.2018-2951, AIAA 2018-2951.

[68] Åström, K. J. and Hägglund, T., *PID Controllers: Theory, Design, and Tuning, Second Edition*, 2nd ed., Instrument Society of America, Research Triangle Park, North Carolina, 1995.

[69] Phillips, C. L., Nagle, H. T., and Chakrabortty, A., *Digital Control System Analysis & Design*, 4th ed., Pearson Prentice Hall, Boston, Massachusetts, 2015.

[70] Nise, N. S., *Control Systems Engineering*, 7th ed., Wiley, Hoboken, New Jersey, 2015.

[71] Kelly, M., "An Introduction to Trajectory Optimization: How to Do Your Own Direct Collocation," *SIAM Review*, Vol. 59, No. 4, 2017, pp. 849–904.
doi: 10.1137/16M1062569.

[72] The MathWorks, Inc., "MATLAB Ver. 9.2 (R2017a)," Natick, Massachusetts, 2017.

[73] The MathWorks, Inc., "MATLAB Optimization Toolbox Ver. 7.6 (R2017a)," Natick, Massachusetts, 2017.

[74] Galles, M. B., Schiller, N. H., Ackerman, K. A., and Newman, B., "Feedback Control of Flight Speed to Reduce Unmanned Aerial System Noise," *Proceedings of the 24th AIAA/CEAS Aeroacoustics Conference*, AIAA Aviation Forum, Atlanta, Georgia, June, 2018.
doi: 10.2514/6.2018-2950, AIAA 2018–2950.

[75] Galles, M. B. and Newman, B., "Reducing the Noise Impact of Small Aircraft through Indirect Trajectory Optimization," *Proceedings of the 26th AIAA/CEAS Aeroacoustics Conference*, AIAA Aviation Forum, Reno, Nevada, June, 2020 (to be submitted).

[76] Gray, J. S., Hwang, J. T., Martins, J. R. R. A., Moore, K. T., and Naylor, B. A., "OpenMDAO: An Open-Source Framework for Multidisciplinary Design, Analysis, and Optimization," *Structural and Multidisciplinary Optimization*, Vol. 59, No. 4, 2019, pp. 1075–1104.
doi: 10.1007/s00158-019-02211-z.

[77] Pascioni, K. A., Rizzi, S. A., and Schiller, N., "Noise Reduction Potential of Phase Control for Distributed Propulsion Vehicles," *Aeroacoustics, AIAA Scitech 2019 Forum*, AIAA, San Diego, California, January, 2019.
doi: 10.2514/6.2019-1069, AIAA 2019-1069.

VITA

Matthew Bruce Galles
Old Dominion University
Department of Mechanical and Aerospace Engineering
238 Kaufman Hall, Norfolk, Virginia 23529

Education

Old Dominion University — Norfolk, Virginia
Bachelor of Science in Mechanical Engineering — December 2014

Tidewater Community College — Virginia Beach, Virginia
Associate of Science in Engineering — August 2012

Professional Experience

Pathways Intern – Structural Acoustics Branch — May 2017 – Present
NASA Langley Research Center — Hampton, Virginia
- Research methods to reduce UAS noise using feedback control.
- Produce conference papers to disseminate results of work to the research community.

Graduate Teaching Assistant — January 2019 – May 2019
Old Dominion University — Norfolk, Virginia
- Managed laboratory sessions for MAE 438/538: Applied Analog & Dgital Controls.
- Assisted students with MATLAB, Simulink, data acquisition, and real time control.

Test Engineer II – Research & Development - Test Group — January 2015 – May 2017
Liebherr Mining Equipment, Newport News Co. — Newport News, Virginia
- Developed hardware-in-the-loop (HIL) testing systems.
- Created automated software tests to reduce testing time and cost.

Engineering Intern – Product Development - Fuel Rails — May 2014 – November 2014
Continental Automotive Systems — Newport News, Virginia
- Designed a cleanliness test fixture & control system for existing fuel rails.
- Lead a greenbelt project to reduce fuel injector assembly time.

Publications

1. Galles, M. B., Schiller, N. H., Ackerman, K. A., and Newman, B., "Feedback Control of Flight Speed to Reduce Unmanned Aerial System Noise," *Proceedings of the 24th AIAA/CEAS Aeroacoustics Conference*, AIAA Aviation Forum, Atlanta, GA, June, 2018. doi: 10.2514/6.2018-2950 AIAA 2018-2950
2. Galles, M. B. and Newman, B., "Reducing the Noise Impact of Small Aircraft through Indirect Trajectory Optimization," *Proceedings of the 26th AIAA/CEAS Aeroacoustics Conference*, AIAA Aviation Forum, Reno, NV, June, 2020 (to be submitted).